Research Paper

Extensive characterization of aerosol optical properties and chemical component concentrations: Application of the GRASP/Component approach to long-term AERONET measurements

Xindan Zhang [a], Lei Li [a,*], Cheng Chen [b,c], Yu Zheng [a], Oleg Dubovik [b], Yevgeny Derimian [b], Anton Lopatin [c], Ke Gui [a], Yaqiang Wang [a], Hujia Zhao [d], Yuanxin Liang [a], Brent Holben [e], Huizheng Che [a], Xiaoye Zhang [a]

[a] State Key Laboratory of Severe Weather (LASW) and Key Laboratory of Atmospheric Chemistry (LAC), Chinese Academy of Meteorological Sciences, CMA, Beijing 100081, China
[b] Univ. Lille, CNRS, UMR 8518 – LOA – Laboratoire d'Optique Atmosphérique, 59000 Lille, France
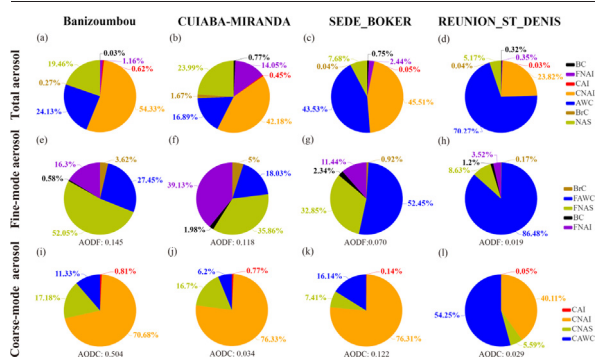[c] GRASP-SAS, Villeneuve d'Ascq, France
[d] Institute of Atmospheric Environment, Shenyang, China
[e] Biospheric Sciences Branch, Code 923, NASA/Goddard Space Flight Center, Greenbelt, MD, USA

HIGHLIGHTS

- A new aerosol component method was applied to sun photometer measurements.
- Component retrievals characterize well the different aerosol types.
- Component retrievals are in line with the physical expectation of optical parameters.
- Aerosol optical retrievals are in good agreement with AERONET standard products.
- Both MG and VW component approaches provide accurate optical property products.

GRAPHICAL ABSTRACT

ABSTRACT

A recently developed GRASP/Component approach (GRASP: Generalized Retrieval of Atmosphere and Surface Properties) was applied to AERONET (Aeronet Robotic Network) sun photometer measurements in this study. Unlike traditional aerosol component retrieval, this approach allows the inference of some information about aerosol composition directly from measured radiance, rather than indirectly through the inversion of optical parameters, and has been integrated into the GRASP algorithm. The newly developed GRASP/Component approach was applied to 13 AERONET sites for different aerosol types under the assumption of aerosol internal mixing rules to analyze the characteristics of aerosol components and their distribution patterns. The results indicate that the retrievals can characterize well the spatial and temporal variability of the component concentration for different aerosol types. A reasonable agreement between GRASP BC retrievals and MERRA-2 BC products is found for all different aerosol types. In addition, the relationships between aerosol component content and aerosol optical parameters such as aerosol optical depth (AOD), fine-mode fraction (FMF), absorption Ångström exponent (AAE), scattering Ångström exponent (SAE), and single scattering albedo (SSA) are also analyzed for indirect verifying the reliability of the component retrieval. It was demonstrated the GRASP/Component optical retrievals are in good agreement with AERONET standard products

* Corresponding author.
  E-mail address: lilei@cma.gov.cn (L. Li).

[e.g., correlation coefficient (*R*) of 0.93–1.0 for AOD, fine-mode AOD (AODF), coarse-mode AOD (AODC) and Ångström exponent (AE); *R* = ~ 0.8 for absorption AOD (AAOD) and SSA; RMSE (root mean square error) < 0.03 for AOD, AODF, AODC, AAOD and SSA]. Thus, it is demonstrated the GRASP/Component approach can provide aerosol optical products with comparable accuracy as the AERONET standard products from the ground-based sun photometer measurements as well as some additional important inside on aerosol composition.

1. Introduction

The composition content of atmospheric aerosols has important influences on their optical properties and radiative effects (Hu et al., 2005), which is of great significance for monitoring and understanding various aspects of the climate and environment (Jin et al., 2019a, 2019b; Ma et al., 2019). Aerosol radiative forcing has been one of the most uncertain factors in assessments of climate change (IPCC, 2013, 2021). For example, there is a large uncertainty in the assessment of the mass concentration and radiative forcing of black carbon (BC) (Perlwitz and Seland, 2009; Schuster et al., 2016; Sato et al., 2003). Therefore, to reduce these uncertainties, there is a need to better characterize the composition of aerosols using observations (Van Beelen et al., 2014). Although the in-situ measurements can provide very detailed information on aerosol composition, using sampling techniques or laboratory analysis can modify aerosol properties. In addition, it is practically impossible to provide information about aerosol properties in the entire atmospheric column and with large spatial coverage using the in-situ measurements only (Bond et al., 1998; Streets et al., 2001). In contrast, the retrieval of aerosol components from remote sensing data carries the advantage of non-contact, instantaneous state detection, and the ability to maintain the natural state of aerosols, thus avoiding the loss of any information during the measurement process.

A variety of aerosol properties parameters can be provided by ground-based observations such as high-precision observations of direct solar light and sky-scattered light. For example, a dataset of aerosol parameters can then be retrieved via the statistical method developed by Dubovik and King (2000), which simultaneously employs all available multi-spectral atmospheric radiance measurements. Global and regional aerosol monitoring networks such as AERONET (Aerosol Robotic Network) (Holben et al., 1998), PHOTONS (Photométrie pour le Traitement Opérationnel de Normalisation Satellitaire) (Goloub et al., 2007), CARSNET (China Aerosol Remote Sensing Network) (Che et al., 2009) and SKYNET (Takamura and Nakajima, 2004) have made significant contributions to the development of ground-based aerosol remote sensing. In recent years, the AERONET algorithm has evolved through three versions (V1, V2 and V3) and V2 has been updated to V3 with improvements to data input and calibration, fully automated cloud screening and instrument anomaly quality control (Giles et al., 2019). The main products of aerosol optical parameters, including aerosol optical depth (AOD), Ångström exponent (AE), single scattering albedo (SSA), size distribution, and complex refractive index, can be provided by AERONET with a high degree of accuracy (Giles et al., 2019). However, AERONET algorithm does not provide aerosol components product.

On the other hand, estimation of aerosol components can be achieved by fitting aerosol optical parameters such as aerosol complex refractive index and SSA. For example, a series of component algorithms were proposed and developed using the AERONET extended aerosol optical parameters. Specifically, Schuster et al. (2005) developed a three-component model for aerosols, including BC, sulphate and water, which uses the differences in real and imaginary parts of the refractive index between BC and aerosol water content (AWC) to estimate their concentrations. Similarly, Dey et al. (2006) and Arola et al. (2011) took advantage of the significant variation in the light absorption of brown carbon (BrC) with wavelength to achieve the retrieval of BrC as well. Subsequently, Wang et al. (2012) added to the Schuster three-component model (Schuster et al., 2005) a dust component that also has strong absorption at short wavelengths. The spectral dependence of the imaginary part of the complex refractive index is similar for dust and BrC, making it difficult to distinguish between

these two absorption components. To address this challenge, Wang et al. (2013) subsequently used the spectral variability of SSA to distinguish between the two components, developed a five-component model including three absorbing components (BC, dust and BrC) simultaneously, and assessed the inversion uncertainty. Then, a more complete model of aerosol components was developed by Van Beelen et al. (2014), and various optical parameters such as complex refractive index, AOD, SSA and sphericity were used jointly to infer the aerosol components. In fact, since SSA is a metric that contains both optical absorption and particle size, these studies therefore implicitly demonstrate the importance of particle size in the estimation of aerosol components. Taking into account the effect of particle size, Schuster et al. (2016) developed a more complex composition model with different components for coarse and fine modes, and further considered the effect of light absorption by dust containing iron oxides on the retrieval of BC, thus minimized the influence on the BC retrieval. Since the differences in the real and imaginary parts of the complex refractive index among various scattering components are quite small, additional information provided by other parameters is needed to identify the scattering component species. The size distribution of particles and spherical particle ratio are helpful to distinguish sea salt from ammonium sulfate and mineral dust, respectively (Van Beelen et al., 2014). It is noted that all the aerosol component algorithms mentioned above estimate the aerosol components in an intermediate step in which they are retrieved from AERONET products (such as the real and imaginary parts of the complex refractive index, SSA, size distribution, etc.), i.e. not directly from the measured radiance. It has been demonstrated that the uncertainties of component retrieval in these intermediate methods are mainly driven by uncertainties in the aerosol optical and microphysical parameters used as input (Schuster et al., 2016). Therefore, uncertainty in the aerosol optical parameters could result in the amplification of uncertainty in the aerosol components estimated by indirect retrieval methods, which could be improved by directly fitting the solar radiation observations for the retrievals of aerosol components and aerosol optical properties together. Based on this idea, a new aerosol component module for the Generalized Retrieval of Atmosphere and Surface Properties (GRASP) algorithm (Dubovik et al., 2011, 2014, 2021) was recently developed for the retrieval of aerosol components directly from remote-sensing data (Li et al., 2019, 2020a). The retrieval uncertainties associated with the employed refractive index for each component were estimated to be 30% for BC, 50% for BrC, 100%–150% for dust or organic carbon (OC), and 70% for iron oxides, based on POLDER/PARASOL observations (Li et al., 2019). It has been demonstrated that the GRASP/Component approach not only provides commonly comparable aerosol optical parameters, but also enables remote monitoring of aerosol components over large spatial and temporal scales (Li et al., 2019, 2020a, 2020b).

Feasibility of the GRASP/Component approach application to AERONET sun photometer measurements was illustrated in (Li et al., 2019), in this study we now apply the GRASP/Component algorithm for a direct estimation of aerosol components from AERONET sun/sky radiance measurements for long-time series and for diferent sites. We also illustrate that the derived optical characteristics are consistent with the standard AERONET optical product.

The paper is organized as follows: Section 2 presents the data and methods used in this study; Section 3 analyzes the characteristics of different aerosol component in different aerosol types and the relationship between the aerosol component content and aerosol optical properties [AOD, fine mode fraction (FMF), absorption AE (AAE), scattering AE (SAE) and SSA], which is also an indirect validation and evaluation of

component retrievals, followed by a comprehensive intercomparison of the aerosol optical parameters [AOD, fine-mode AOD (AODF), coarse-mode AOD (AODC), absorption AOD (AAOD), SSA, AE] between GRASP/Component approach and the corresponding AERONET standard products during the period 2014–2019; and finally, in Section 4, the main conclusions are presented.

2. Data and methods

2.1. AERONET measurement

AERONET is a global network of ground-based multi-spectral sun/sky photometers (Holben et al., 1998, 2001). The radiometers automatically provide direct measurements of solar radiation (nominally centered at 340, 380, 440, 500, 670, 870, 940, 1020, and 1640 nm), which can be processed to obtain AOD. In addition, sky radiance is measured at four wavelengths (440, 675, 870 and 1020 nm) by combination with almucantar and principal plan scans (in some locations sky-radiance measurements are also available at other wavelengths). Many aerosol optical and microphysical parameters can be derived from sky radiance measurements (Dubovik and King, 2000; Dubovik et al., 2000). The AERONET aerosol dataset consists of three quality levels: Level 1.0 for non-cloud-screened data, Level 1.5 for cloud-screened data, and Level 2.0 for cloud-screened and quality-assured data. Based on the measured solar radiance, the AERONET algorithm can provide the aerosol properties in real time, such as multi-wavelength AOD products with high temporal resolution and highly reliable accuracy ($\sim \pm 0.01$ to ± 0.02) (Eck et al., 1999). Strict calibration and maintenance protocols are conducted to ensure consistency between instruments, which is helpful for providing high-quality aerosol products that contribute to the establishment and validation of satellite retrieval algorithms (Levy et al., 2007; Lyapustin et al., 2018; Bréon et al., 2011; Mao et al., 2019; Mélin et al., 2010; Remer et al., 2005; Kahn et al., 2010; Ahn et al., 2014; Kumar et al., 2015).

The AERONET sites used in this study are grouped into five categories based on the classification of aerosol types in the AERONET climatology (Dubovik et al., 2002; Giles et al., 2012) and some existing literature (see Fig. 1), as follows: (a) Biomass Burning (BB) (Holben et al., 2001; Dubovik et al., 2002), typical sites such as the CUIABA-MIRANDA site in central South America, which is affected by a variety of biomass burning

aerosols from cerrado vegetation, agricultural land, tropical forests, etc. during the annual burning season (generally August–September); (b) Dust (DU) (Holben et al., 2001), a typical dust site, Banizoumbou, is located in Niger, north of the Sahara, and is affected by the seasonal wind Harmattan, which brings dust from the Sahara desert region to the area; (c) Marine (MA) (Mallet et al., 2018), considering that sea-air interactions play a key role in the atmospheric system and that the ocean is a reservoir of sea spray aerosols, a typical marine site REUNION_ST_DENIS in the Southern Indian Ocean was chosen for the study of the optical properties and chemical composition of aerosols; (d) Dust_Pollution (DP), representing desert dust predominance with urban/industrial pollution transports (Derimian et al., 2006). Here we chosen the Sede_Boker site in the Negev desert in Israel, which is heavily affected by dust from April to May and mainly by urban/industrial pollution from July to August; and (e) Multi-source Urban (MU), representing a variety of different aerosol sources in an urban background (Dubovik et al., 2002; Bergamo et al., 2008; Mitchell et al., 2013; Kabashnikov et al., 2014; Chubarova et al., 2011; Eck et al., 2005; Giannakaki et al., 2010). Level 2 total optical depth data and Level 2 almucantar data are downloaded from the AERONET website to prepare the input data for the GRASP/Component approach. The measured data at these AERONET sites are processed by the GRASP/Component approach for the aerosol component and optical properties retrievals. Meanwhile, the AERONET V3 Level 2.0 quality-assured products (http://www.aeronet.gsfc.nasa.gov; last accessed 7 April 2021) (Giles et al., 2019) were used to validate the GRASP/Component aerosol optical retrievals from sun photometer measurements.

2.2. MERRA-2 data

The Modern-Era Retrospective Analysis for Research and Applications, Version 2 (MERRA-2) is a re-analysis dataset with global coverage of long time series that begins in 1980, with a spatial resolution of $0.5° \times 0.625°$ and a temporal resolution of 1 h. MERRA-2 uses an upgraded version of the Goddard Earth Observing System model, Version 5 (GEOS-5) data assimilation system to replace the original MERRA reanalysis. Compared to the MERRA-1, MERRA-2 offers a number of improvements that reflected throughout the period of aerosol assimilation (Molod et al., 2015; Rienecker et al., 2008, 2011). The aerosols in MERRA-2 were simulated
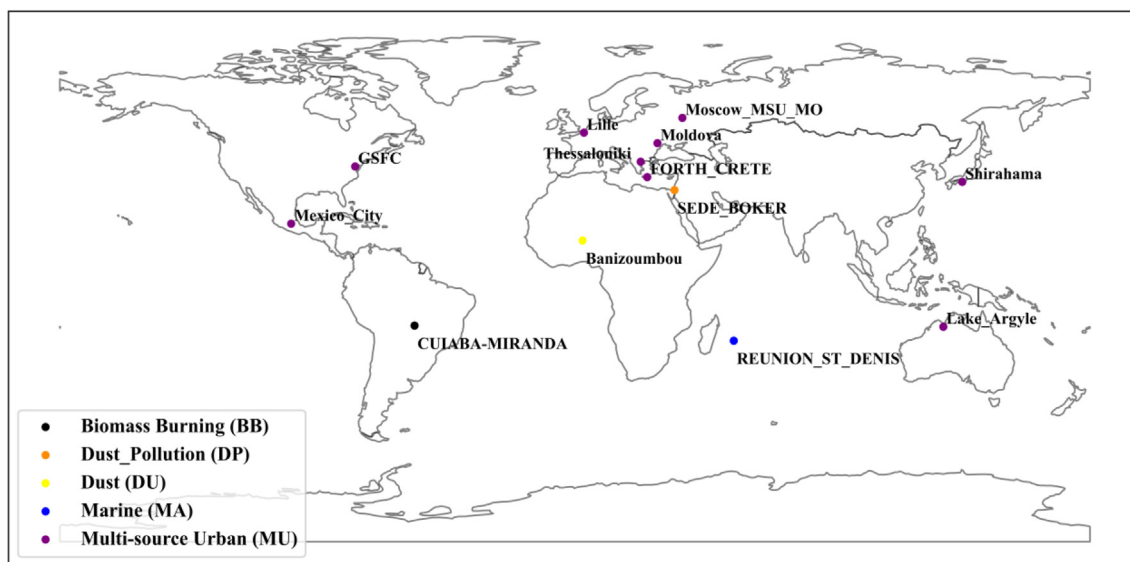

Fig. 1. Geographical distribution of the AERONET sites used in this study. The colors of sites are associated with the main aerosol types as: (a) Biomass Burning (BB); (b) Dust (DU); (c) Marine (MA); (d) Dust_Pollution (DP), representing dust and pollution events occurring alternately; and (e) Multi-source Urban (MU), representing a variety of different aerosol sources in an urban background.

by coupling the GEOS-5 model with the Goddard Chemistry, Aerosol, Radiation, and Transport (GOCART) (Chin et al., 2002; Colarco et al., 2010) aerosol module to take into account the estimation of the source, sink and chemical components of the aerosols. Here we employ MERRA-2 monthly mean BC concentration (2015–2019) to validate our BC products derived by the component approach.

2.3. GRASP/component approach

The GRASP algorithm is a highly rigorous and versatile algorithm for the enhanced characterization of aerosol properties from a diverse range of remote sensing data such as sun photometers, lidar, satellite observations, etc. (Dubovik et al., 2014, 2021; Torres et al., 2017; Titos et al., 2019; Hu et al., 2019; Tsekeri et al., 2017), and is available at https://www.grasp-open.com. The multi-term least-squares method (LSM) was employed in the GRASP algorithm to achieve a statistically optimal fit to measurements (Dubovik et al., 2021). A detailed description of the GRASP algorithm can be found in Dubovik et al. (2011, 2014, 2021). As described in the study of Dubovik et al. (2021), the GRASP package can be considered as a platform for developing, testing and refining novel retrieval concepts and their utilization in operational processing environments. The aerosol component module was developed and incorporated into the GRASP algorithm with detailed descriptions in Li et al. (2019, 2020a, 2020b). The GRASP/Component approach employs a specific component module that aerosol mixture particles are made up of multiple components internal mixing with known complex refractive index of each component and values of the aerosol mixture complex refractive index are estimated by the fraction of each component together with its refractive index under a certain effective medium approximation mixing rules on aerosol components. Thus, the GRASP/Component approach can directly invert the content of different aerosol components instead of the spectral dependence of the complex refractive index, and directly infer the aerosol component from the measured radiation (such as sun photometer measurements), avoiding the uncertainties associated with intermediate steps for the component estimations (Li et al., 2019), which has been successfully applied to POLDER-3/PARASOL observations. Here, we provide a general description of the GRASP/Component approach for the ground-based AERONET sun photometer measurements.

The description of GRASP/Component products derived from AERONET sun photometer measurements together with AERONET standard products are listed in Table 1. In the GRASP/Component approach,

Table 1

Intercomparison of aerosol products derived by the GRASP/Component from AERONET sun photometer measurements and AERONET standard products. *f* and c indicate fine- and coarse-mode aerosol, respectively. The main differences are in bold.

Retrieval data products	GRASP/component retrievals		AERONET retrievals	
	Total only	Total/fine/coarse	Total only	total/fine/coarse
AOD	No	Yes	No	Yes
AE	No	Yes	No	Yes
SSA	No	Yes	No	Yes
AAOD	No	Yes	No	Yes
AAE	No	Yes	No	Yes
Refractive Index	**No**	Yes (f, c)	**Yes**	**No**
Asymmetry Factor	No	Yes	No	Yes
Sphere Fraction	Yes	No	Yes	No
Size Distribution	**No**	f: 15 bins; c: 10 bins	Yes (22 bins)	**No**
BC	No	**Yes (f)**	No	**No**
BrC	No	**Yes (f)**	No	**No**
NAI	No	**Yes (f, c)**	No	**No**
CAI	No	**Yes (c)**	No	**No**
NAS	No	**Yes (f, c)**	No	**No**
AWC	No	**Yes (f, c)**	No	**No**

differentiating aerosol components by coarse and fine modes allows aerosol components with similar spectral absorption properties to be distinguished (Schuster et al., 2016; Li et al., 2019), e.g., BrC and iron oxides (hematite and goethite) have similar spectral absorption properties (Chen and Cahan, 1981; Chen and Bond, 2010; Schuster et al., 2016). Considering that aerosol particles containing carbon dominate the fine mode, while dust containing iron are mainly distributed in the coarse mode, the GRASP/Component approach therefore classifies BC and BrC as absorbing insoluble components in the fine-mode state, while iron oxides are classified as absorbing insoluble components in the coarse-mode state. In addition, the fine-mode non-absorbing insoluble species (FNAI) are included under the fine mode to represent mainly fine dust or non-absorbing OC, and fine-mode non-absorbing soluble species (FNAS) to represent inorganic salts and fine-mode AWC (FAWC). In the coarse mode, the absorbing insoluble species (CAI) is the only absorptive component and represents mainly iron oxides, in addition to a number of other absorptive elements. The non-absorbing insoluble species (CNAI), mainly representing dust, but also non-absorbing insoluble OC particles. Coarse-mode non-absorbing soluble species (CNAS) represent inorganic salts. In addition to this, the coarse-mode also contains AWC (CAWC).

2.4. Statistical metrics for intercomparison

Standard statistical parameters including Pearson's linear correlation coefficient (R), root-mean-square error (RMSE), mean absolute error (MAE), mean relative error (MRE), slope and offset of linear regression are used to evaluate the intercomparison:

$$R = \frac{\sum_{i=1}^{N}\left(X_{i,AERONET} - \bar{X}_{i,AERONET}\right)\left(X_{i,GRASP} - \bar{X}_{i,GRASP}\right)}{\sqrt{\sum_{i=1}^{N}\left(X_{i,AERONET} - \bar{X}_{i,AERONET}\right)^2 \sum_{i=1}^{N}\left(X_{i,GRASP} - \bar{X}_{i,GRASP}\right)^2}}, \quad (1)$$

$$RMSE = \sqrt{\frac{\sum_{i=1}^{N}\left(X_{i,GRASP} - X_{i,AERONET}\right)^2}{N}}, \quad (2)$$

$$MAE = \frac{1}{N}\sum_{i=1}^{N}\left|X_{i,AERONET/GRASP} - X_{i,MERRA}\right| \quad (3)$$

$$MRE = \frac{1}{N}\sum_{i=1}^{N}\left|\frac{X_{i,AERONET/GRASP} - X_{i,MERRA}}{X_{i,AERONET/GRASP}}\right| \times 100\% \quad (4)$$

where N is the number of matched data points, X_{GRASP} represents the retrieval of the GRASP/Component approach, $X_{AERONET}$ represents the standard AERONET, and $\bar{X}_{GRASP}$ and $\bar{X}_{AERONET}$ represent the average of the GRASP/Component retrievals and AERONET products, respectively. X_{MERRA} and $X_{AERONET/GRASP}$ represents the MERRA-2 BC products and GRASP BC retrievals inverted from AERONET, respectively.

3. Results and discussion

3.1. Aerosol component retrievals

The approach provides both the information about absolute concentration of aerosol and the distribution of the aerosol volume among different components. The presence of different component is assumed different in fine and coarse aerosol modes as described in Li et al. (2019).

3.1.1. Volume concentrations of aerosol components

We present the distribution characteristics of aerosol component concentrations for different aerosol types in 2017 (Fig. 2) because we consider that the measurements of each aerosol type site should have a good temporal coverage during the whole year, in particular for the Biomass Burning site where there are usually not enough observations during the biomass burning season. It can be seen that in Fig. 2 the highest volume concentration of BC (1.83 mm³/m²) is found at Biomass Burning site, followed by
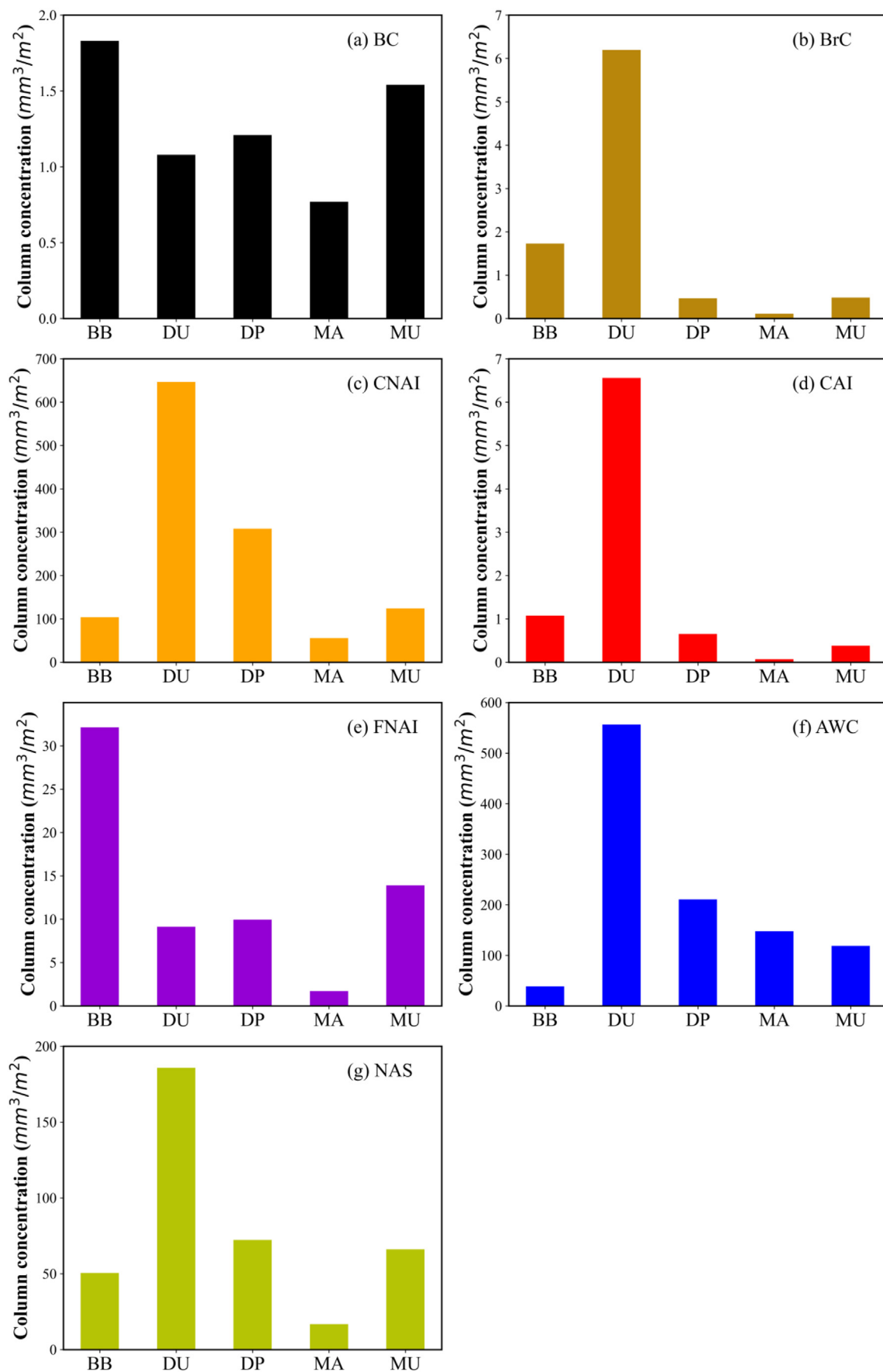
Fig. 2. Yearly average volume concentration of aerosol components for five different aerosol types: (a) Biomass Burning (BB); (b) Dust (DU); (c) Marine (MA); (d) Dust_Pollution (DP); and (e) Multi-source Urban (MU).

relatively high volume concentrations of BC at Multi-source Urban (1.54 mm³/m²) and Dust_Pollution (1.21 mm³/m²) sites, which is consistent with the fact that BC is mainly emitted from biomass burning and fossil fuel combustion. The volume concentrations of CNAI are much higher than other aerosol components for all different aerosol types, in particular for pure Dust sites. Specifically, the maximum concentration of retrieved CNAI was found at Dust site (646.51 mm³/m²), which was twice as high as the Dust_Pollution site and 6–12 times higher than the rest of other sites, indicating a significant contribution of scattering dust particles to the aerosol loading at DU site. Similarly, CAI concentration at the Dust site (6.56 mm³/m²) is several times higher than that in other aerosol types (Biomass Burning: 1.08 mm³/m², Dust_Pollution: 0.65 mm³/m², Marine: 0.07 mm³/m², Multi-source Urban: 0.38 mm³/m²), thus revealing the contribution of absorbing dust particles (mainly iron oxides) to aerosol loading at the Dust site. The relatively high concentrations of BC and CNAI are observed at the Dust_Pollution site because dust and urban/industrial pollution aerosols dominate at this site. The highest concentration of FNAI is observed at Biomass Burning site, followed by Multi-source Urban and Dust_Pollution sites. Based on the assumption and definition of FNAI in this aerosol component approach, high FNAI concentration at the Biomass Burning site can be interpreted as fine-mode scattering organic carbon (i.e., OC) generated from biomass burning, while high FNAI concentration at the Dust site can be interpreted as fine-mode scattering dust particles, which could be post-classified by the AE parameter as well (Li et al., 2019). Similarly, the retrieved FNAI at the Multi-source Urban and Dust_Pollution sites can be considered as a mixture of scattering organic carbon and scattering dust particles. Except AWC component (147.64 mm³/m²), low component concentrations (BC: 0.77 mm³/m², BrC: 0.11 mm³/m², CNAI: 55.64 mm³/m², CAI: 0.07 mm³/m², FNAI: 1.71 mm³/m², NAS: 16.81 mm³/m²) obtained at the Marine site are

attributed to the very low aerosol loading and high relative humidity over ocean. On the contrary, high AWC concentration is also observed at the Dust site because many large particles could provide more opportunities and space to be surrounded by water even for the low aerosol water fraction (in Fig. 3). For NAS results, it is also a similar situation. In addition, soluble organic carbon emitted from biomass burning and soluble mineral salts contained in dust particles are regarded as NAS component as well. Same as BC component, high BrC concentration is observed at Biomass Burning site. However, it is noted that high BrC is also obtained at the Dust site, which is mainly attributed to the contributions of iron oxides (hematite and goethite) absorption in the fine-mode dust particles. Due to the similar spectral absorption of BrC and iron oxides (hematite and goethite), the fine-mode absorbing dust at the Dust site could be misjudged as BrC in the current component approach (Li et al., 2019, 2020a). Such limitations of this component retrieval method could be addressed in future by including some measured information at more wavelengths (such as UV or IR bands).

3.1.2. Volume fractions of aerosol components

Fig. 3 shows the characteristics of aerosol component fractions in the fine- and coarse-mode as well as fractions in total aerosol. Considering the quite different values of aerosol loading in fine- and coarse-mode aerosol particles for different aerosol types, the component retrievals in very low aerosol loading cases could have large uncertainties such as coarse-mode component retrievals in biomass burning sites (AODC is very low). We chose retrievals in June at Banizoumbou site to represent dust aerosol, in October at CUIABA-MIRANDA site to represent biomass burning aerosol, in April at SEDE-BOKER site to represent a mixture of dust and urban/industrial pollution aerosol, and in March at REUNION_ST_DENIS site to represent marine aerosol. It can be seen that the AODC at 675 nm at Banizoumbou site (0.504) is much higher than other aerosol type sites
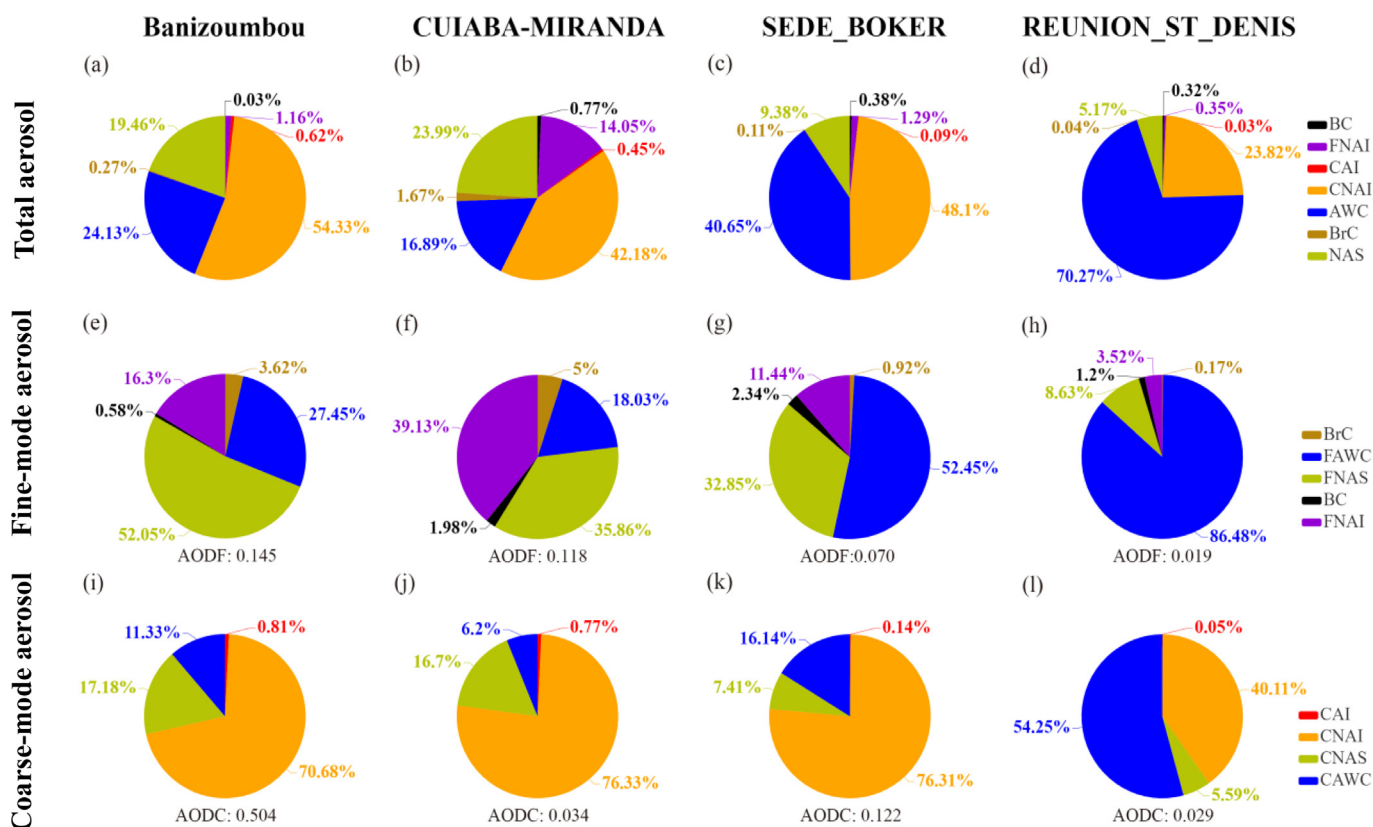

Fig. 3. Examples of monthly average aerosol component volume fractions inversion using the GRASP/Component approach: (a, e, i) present component fractions at Banizoumbou site for dust type in June; (b, f, j) present component fractions at CUIABA-MIRANDA site for biomass burning type in October; (c, g, k) present component fractions at SEDE_BOKER site for dust and pollution mixing type in April; (d, h, l) presents component fractions at REUNION_ST_DENIS site for marine aerosol type in March. The values of AODF and AODC at 675 nm are also provided in the figure.

(CUIABA-MIRANDA: 0.034, SEDE_BOKER: 0.122, REUNION_ST_DENIS: 0.029) due to the predominance of dust. Corresponding to high AODC, the dust aerosol at Banizoumbou site has the highest CNAI volume fraction (54.33%) compared to other aerosol types (CUIABA-MIRANDA: 42.18%, SEDE_BOKER: 48.1%, REUNION_ST_DENIS: 23.82%) in the total aerosol fraction, and the CNAI volume fraction can be up to 70.68% in the coarse-mode aerosol fraction, indicating a significant contribution of scattering dust particles to the aerosol loading for dust aerosol at Banizoumbou site. Similarly, CAI fraction at the Banizoumbou site (0.62%) is several times higher than that at other aerosol type sites (CUIABA-MIRANDA: 0.45%, SEDE_BOKER: 0.09%, REUNION_ST_DENIS: 0.03%), revealing the contribution of absorbing dust particles in dust aerosol at the Banizoumbou site. Unlike other aerosol type sites where AODC is larger than AODF, the AODF at CUIABA-MIRANDA site (0.118 at 675 nm) is much higher than AODC (0.034 at 675 nm), indicating that CUIABA-MIRANDA site is dominated by fine-mode aerosols. The highest volume fractions of BC and BrC (0.77%, 1.67% in total aerosol fraction, respectively) are found in the biomass burning aerosol at CUIABA-MIRANDA site, which is much higher than that in other aerosol type cases (Banizoumbou: 0.03%, 0.27% in total aerosol fraction; SEDE_BOKER: 0.38%, 0.11% in total aerosol fraction;

REUNION_ST_DENIS: 0.32%, 0.04% in total aerosol fraction). High fractions of BC and BrC observed at CUIABA-MIRANDA site present a significant contribution of light-absorbing carbon (BC and BrC) in the biomass burning aerosol. In addition, the SEDE_BOKER site representing a mixing type of dust and urban/industrial pollution has large fraction of BC (2.34%) in fine-mode aerosol and large fraction of CNAI (76.31%) in coarse-mode aerosol. It is noted that fine-mode absorbing dust at Banizoumbou site could be misinterpreted as a contribution of BrC fraction in fine-mode aerosol. The highest volume fraction of AWC was retrieved at REUNION_ST_DENIS site, a typical marine site, that the AWC accounted for 70.27% in total aerosol, 86.48% in fine-mode aerosol, and 54.25% in coarse-mode aerosol. The component retrievals at REUNION_ST_DENIS site may have large uncertainties because of very low aerosol loading (AODF: 0.019 and AODC: 0.029).

3.1.3. Relationship between aerosol optical properties and aerosol components

In order to validate the applicability of the GRASP/Component approach for aerosol component retrieval, the relationship between aerosol component retrievals and aerosol optical retrievals are discussed in this section. We can see that the trend of annual average aerosol component
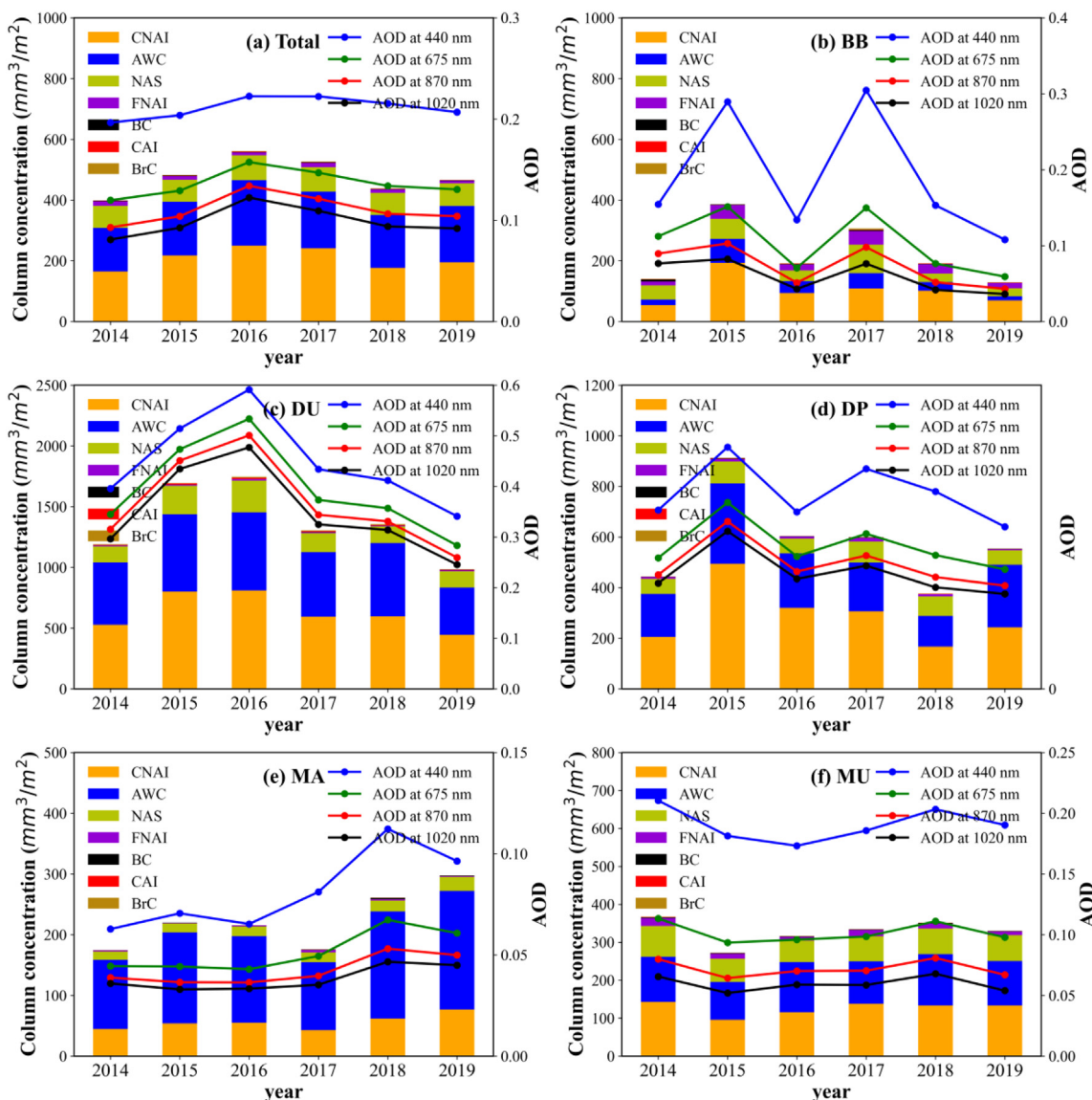

Fig. 4. Yearly average volume concentration of aerosol components and AOD for all different aerosol types and in total: (a) Total; (b) Biomass Burning (BB); (c) Dust (DU); (d) Marine (MA); (e) Dust_Pollution (DP); and (f) Multi-source Urban (MU).

concentration is the same as the trend of AOD for all sites as well as for each aerosol type (in Fig. 4). Figs. 5 and 6 show the trends of monthly average component concentrations (BC, BrC, FNAI, CANI, and CAI) and FMF at a typical Dust site (Banizoumbou) and Biomass Burning site (CUIABA-MI-RANDA), respectively. At the Dust site (Fig. 5), the FMF is usually less than 60% and in March–July the FMF is about 40% or less. At the same time, high volume concentration of CNAI and CAI are apparent in March to June and reach a maximum (1113.79 mm³/m² for CNAI and 14.78 mm³/m² for CAI) in June at Banizoumbou, suggesting that spring and early summer are periods of high dust outbreaks. The monthly average concentration of BC and BrC follow the same trend as FMF, while FNAI sometimes shows an opposite trend. Therefore, the total of BC, BrC and FNAI volume concentration (Fig. 5d) show an opposite trend to FMF, suggesting that the FNAI at Banizoumbou links strongly to CNAI and it could be mainly fine-mode non-absorbing dust. Finally, when the FNAI concentration is high, the CNAI concentration is also very high and the change of FMF is uncertain. At the Biomass Burning site (Fig. 6), the FMF is above 80% in all months except March and April (75% for March and 79% for April), indicating that the aerosol at CUIABA-MIRANDA is dominated by fine-mode particles. The trend of BC concentration follows much similar pattern as FMF with maximum BC concentration (2.92 mm³/m²) and the FMF value (larger than 90%) in October, which is also in a similar

case for BrC retrieval. It is noteworthy that the relationships of FMF to FNAI (Fig. 6c) and CNAI (Fig. 6e) are indefinite, which is probably attributed to the fact that FNAI mainly represents fine-mode non-absorbing OC particles, CNAI mainly represent coarse-mode non-absorbing dust particles and their changes have no associated relationship.

As shown in Fig. 7, we also analyzed the relationship between the absorbing aerosol components (BC, BrC and CAI) and AAE (440/870), and the scattering aerosol components (CNAI, NAS and FNAI) with SAE (440/870) and SSA, for different aerosol types, respectively. The AAE is usually considered to be related to absorbing aerosol components, e.g., pure BC with strong absorption in all wavelengths has a theoretical AAE value of 1. We can see that the AAE is larger than 2.0 at the Dust site and the AAE values for Biomass Burning, Dust_Pollution and Multi-source Urban sites are all above 1.2 (in Fig. 7a), which is consistent with previous studies that for the absorbing components from biomass burning and/or fossil fuel combustion, the AAE is considered to be greater than 1.1, with dust regions having AAEs ranging from 2.0 to 3.0 (Giles et al., 2012; Wang et al., 2016; Bahadur et al., 2012; Lack and Cappa, 2010; Russell et al., 2010). The lowest AAE value is close to 1.0 observed at the Marine site, which is related to the fact that the absorbing component at the Marine site is mainly BC. SAE (usually ranging from 0 to 4) is an important parameter for identifying the size of aerosol particles, that is, small values indicates a
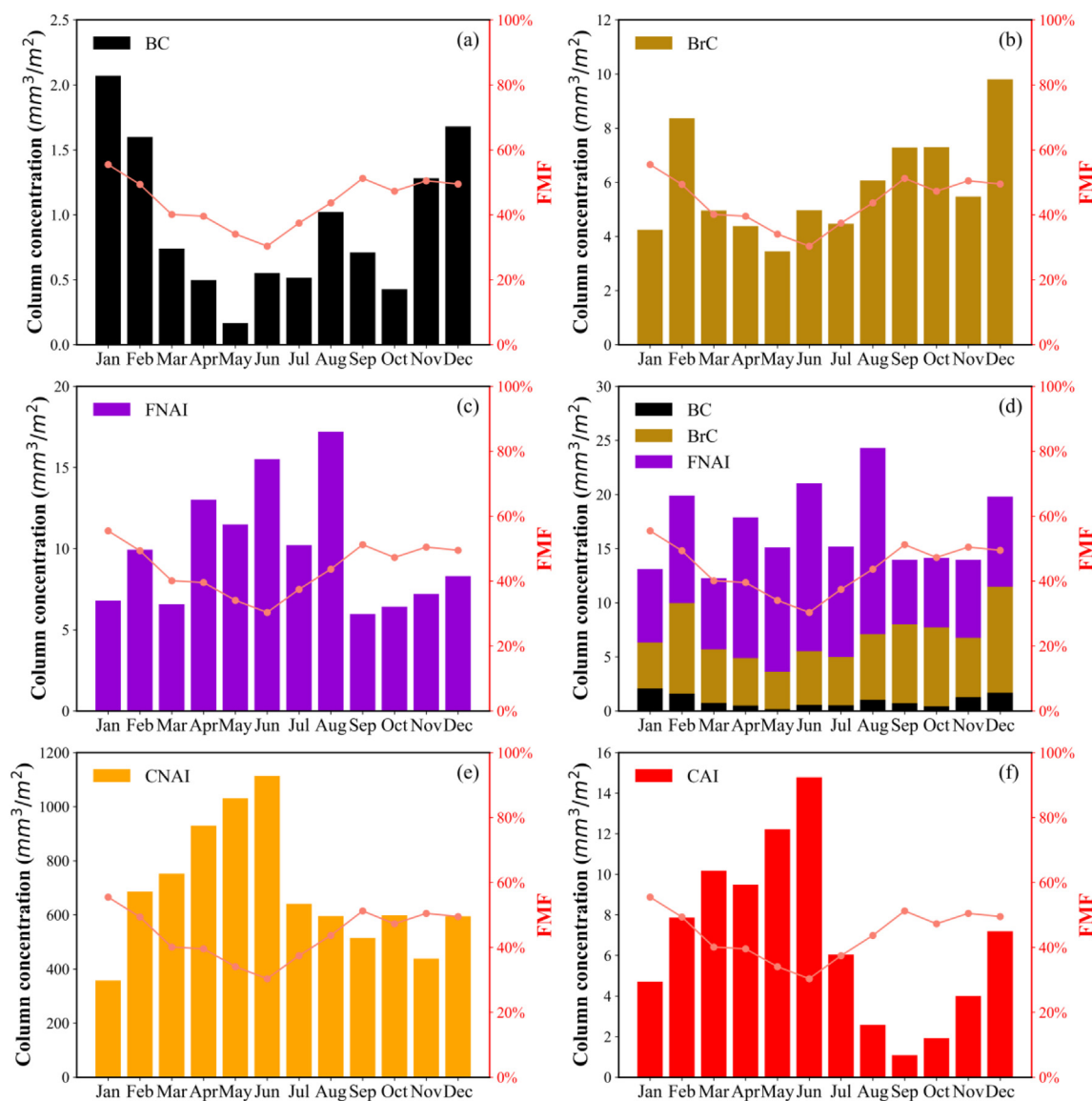

Fig. 5. Monthly average volume concentration of aerosol components and fine-mode fraction (FMF) at Banizoumbou for the period 2014–2019.
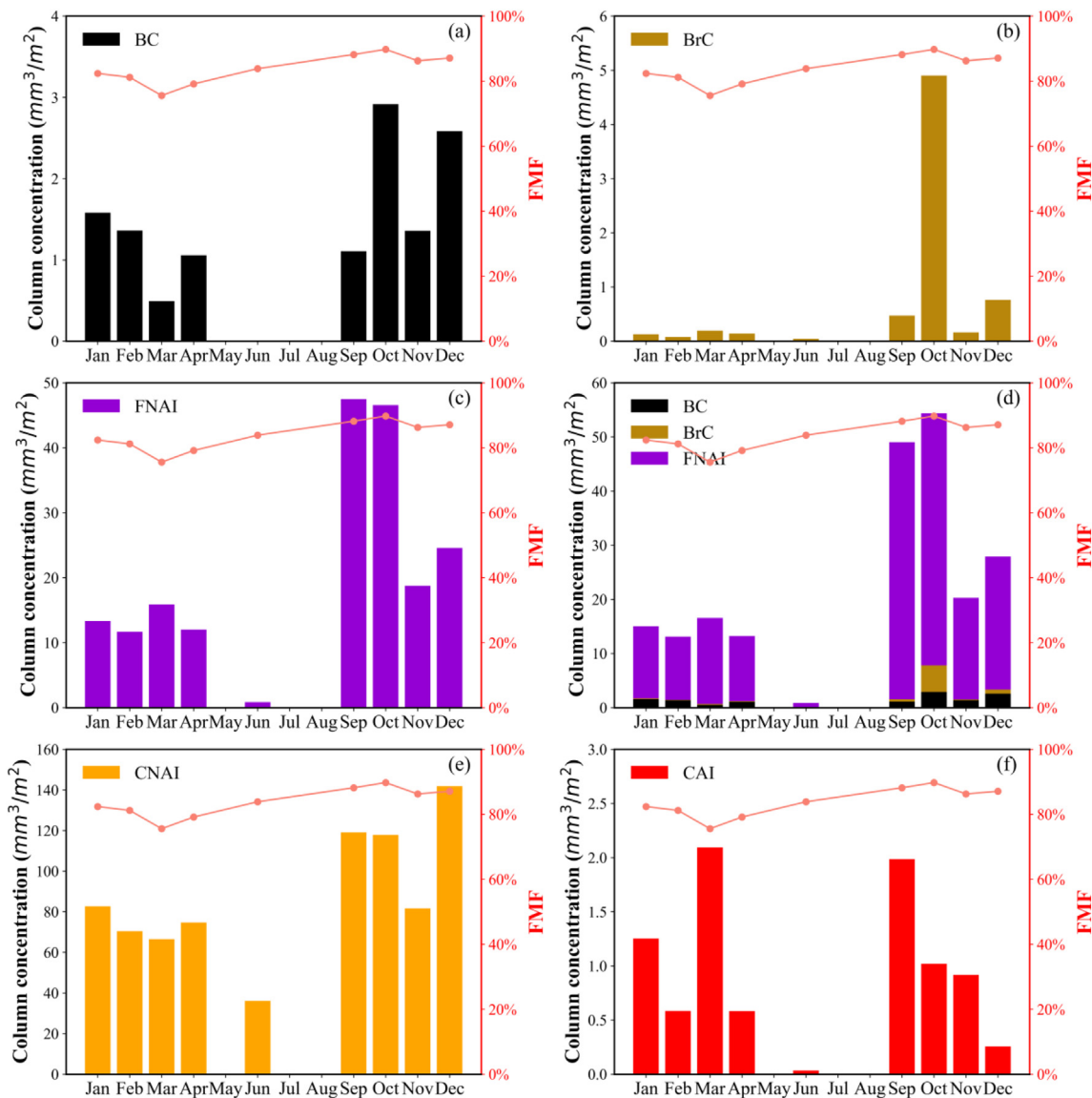
Fig. 6. Monthly average volume concentration of aerosol components and fine-mode fraction (FMF) at CUIABA-MIRANDA for the period 2014–2019.

dominance of coarse particles and large values indicates a dominance of fine particles (Bergstrom et al., 2007; Russell et al., 2010; Cazorla et al., 2013). As shown in Fig. 7b, the lowest SAE values (smaller than 0.4) among all types of aerosol sites are found at the Dust site with high CNAI concentration (more than 600 mm3/m2), followed by the

Dust_Pollution site, indicating that aerosol particles at Dust site are dominated by the coarse mode. Meanwhile, the Biomass Burning and Multi-source Urban sites have the highest SAE values (larger than 1.4), indicating that they are dominated by fine-mode particles. SSA is not only related to the relative content of absorbing components, but
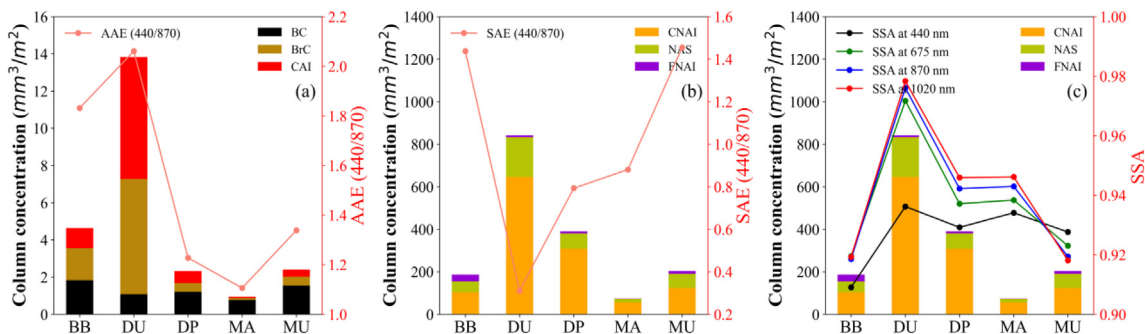

Fig. 7. The relationship between absorbing components (BC, BrC, and CAI) volume concentration and AAE (a), scattering components (CNAI, NAS, and FNAI) volume concentration and SAE (b), and SSA (c) in five different aerosol types: Biomass Burning (BB), Dust (DU), Marine (MA), Dust_Pollution (DP), and Multi-source Urban (MU) for the period 2014–2019.

also influenced by the aerosol particle size (Jacobson, 2001). Fig. 7c shows the relationship between the volume concentration of the scattering aerosol components and SSA. The trend for the concentration of the scattering components is basically the same as that of SSA, e.g., the highest volume concentration of the scattering component and the highest SSA value are obtained at the Dust site, and medium SSA values at the Marine site are linked to the concentration of the scattering components, which is related to the predominantly coarse mode of the aerosol particles in marine areas (Chen et al., 2020). The smallest SSA values are observed at Biomass Burning and Multi-source Urban sites, where there are many absorbing matters/components emitted from biomass burning or fossil fuel combustion.

Fig. 8 shows the distribution of different aerosol types as a function of AAE and SAE together with aerosol component retrievals derived by the GRASP/Component approach from sun photometer measurements. The colour coding of the data points was determined by the BC and CNAI volume concentration, BC/(BC + BrC) ratio, and the ratio of the absorbing component concentration to the total component volume concentration, respectively. As the AAE value increases and the SAE value decreases, the BC content decreases (Fig. 8a) and the CNAI content increases (Fig. 8b) at the Dust site, which is consistent with the findings of Yang et al. (2009) that dust-type aerosols have an SAE close to 0 owing to their large particle sizes and variable AAE values (~ 1.2 to 3) (Dubovik et al., 2002). At the Dust_Pollution site, the range of SAE values is large (~ 0.2 to 1.4) owing to the wide range of particle sizes across the various shapes, and AAE values range from 1 to 2 with high BC concentration (Fig. 8a) and the value of BC/

(BC + BrC) close to 1 (Fig. 8c) when the AAE is close to 1. As shown in Fig. 8d, the Biomass Burning site has the largest proportion of absorbing components with a high BC proportion in sum of BC and BrC (see Fig. 8c). At Multi-source Urban sites, the range of variation in AAE and SAE is small with data points concentrated between 1.1 and 1.2 for AAE and between 1.3 and 1.8 for SAE, indicating a predominance of fine particles. The closer the AAE value is to 1, the higher the BC/(BrC + BC) value (see Fig. 8c). At the Marine site, the SAE values have a large span and the AAE values are close to 1, which is related to the high proportion of BC in sum of BC and BrC at the Marine site. In parallel with the results of Russell et al. (2010), AAE values at Multi-source Urban sites are close to 1, larger AAE values for Biomass Burning site, and the largest AAE values for Dust site. Overall, the aerosol component results derived by the GRASP/Component approach from sun photometer measurements have been demonstrated and validated using the aerosol optical property retrievals (AOD, FMF, AAE, SAE and SSA).

3.2. Validation

3.2.1. Comparison of GRASP/component BC retrieval and MERRA-2 BC products

To validate the reliability of the GRASP/Component retrieval results, the MERRA-2 BC data were selected to compare with the BC column mass concentration inverted by the GRASP/Component approach from AERONET sun photometer measurements in this study. For the spatial matching of MERRA-2 to AERONET sites, a
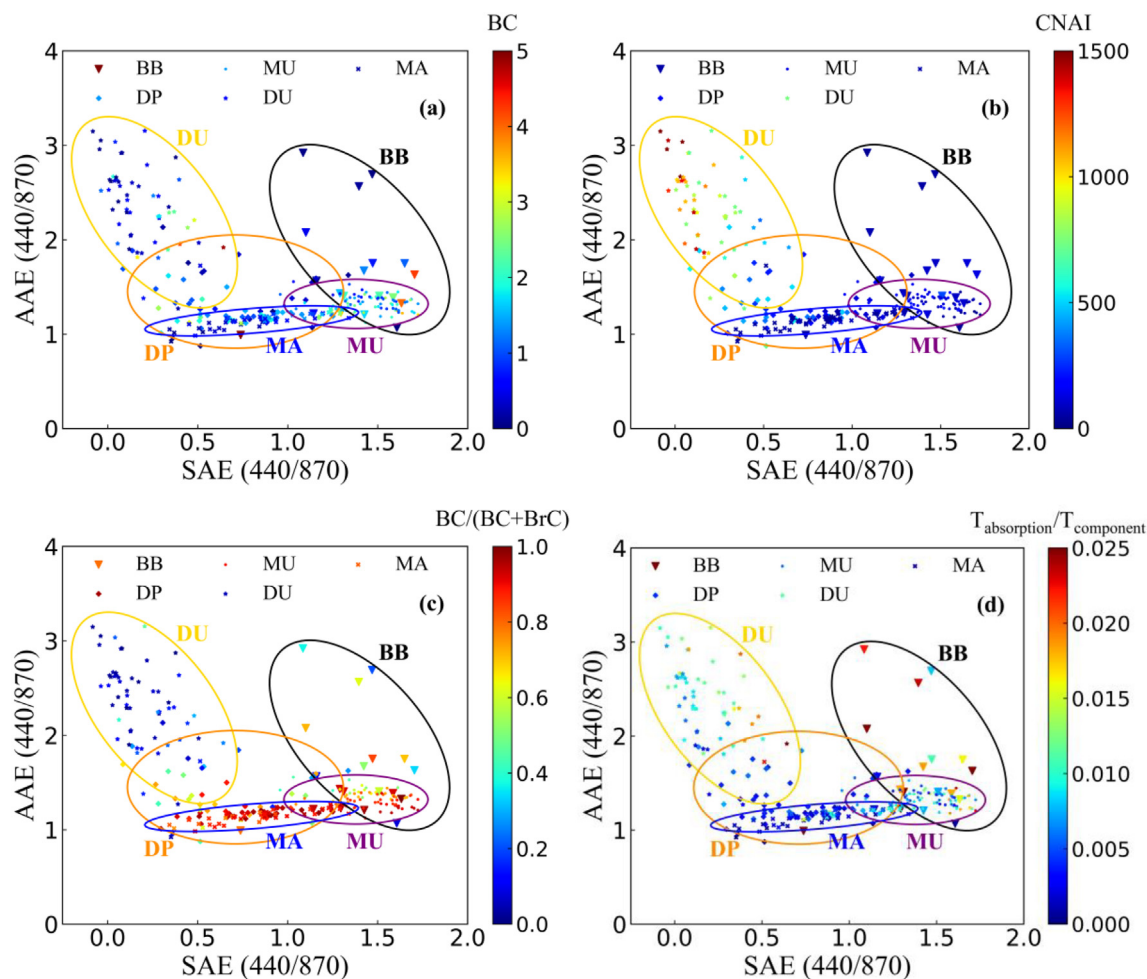

Fig. 8. The distribution of different aerosol types as a function of AAE and SAE together with aerosol component retrievals derived by the GRASP/Component approach from sun photometer measurements. The colors of monthly average retrievals are linked to the colour-bar values. $T_{\text{absorption}}$ indicates the volume concentration of the absorbing component; $T_{\text{component}}$ indicates the volume concentration of all components.
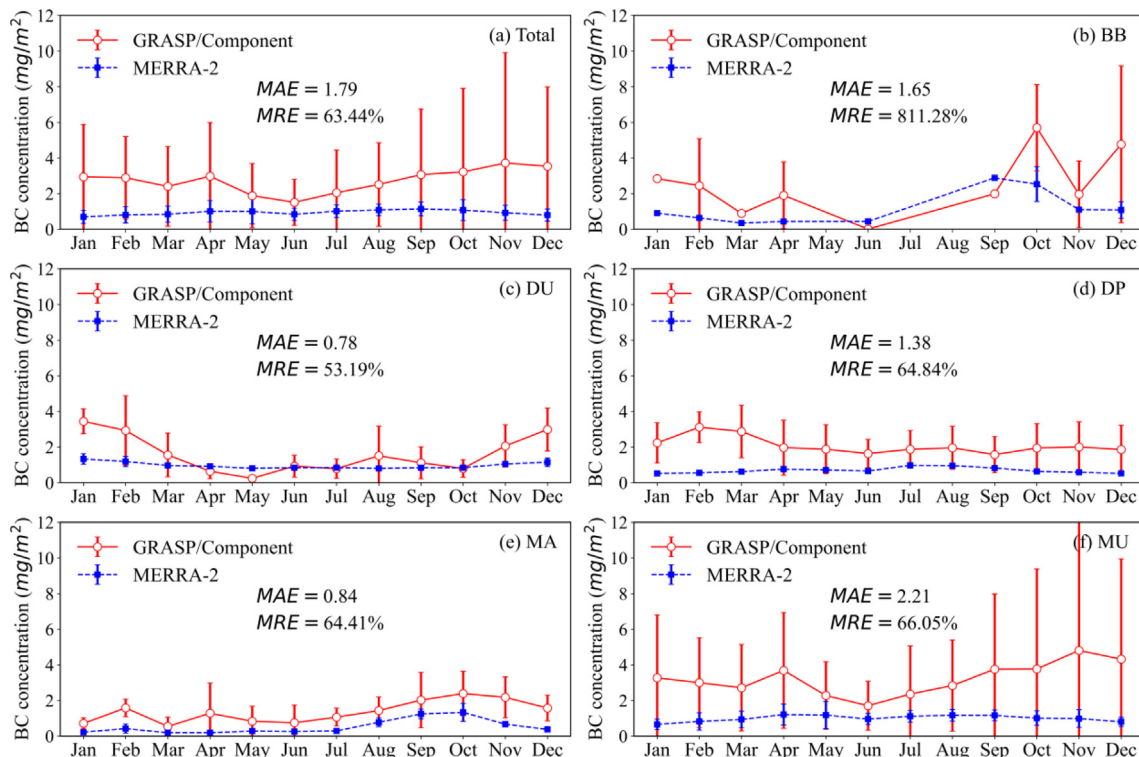
Fig. 9. Intercomparison between the monthly average BC concentration derived by the MERRA-2 and GRASP/Component approach for all different aerosol types and in total: (a) Total; (b) Biomass Burning (BB); (c) Dust (DU); (d) Marine (MA); (e) Dust_Pollution (DP); and (f) Multi-source Urban (MU).
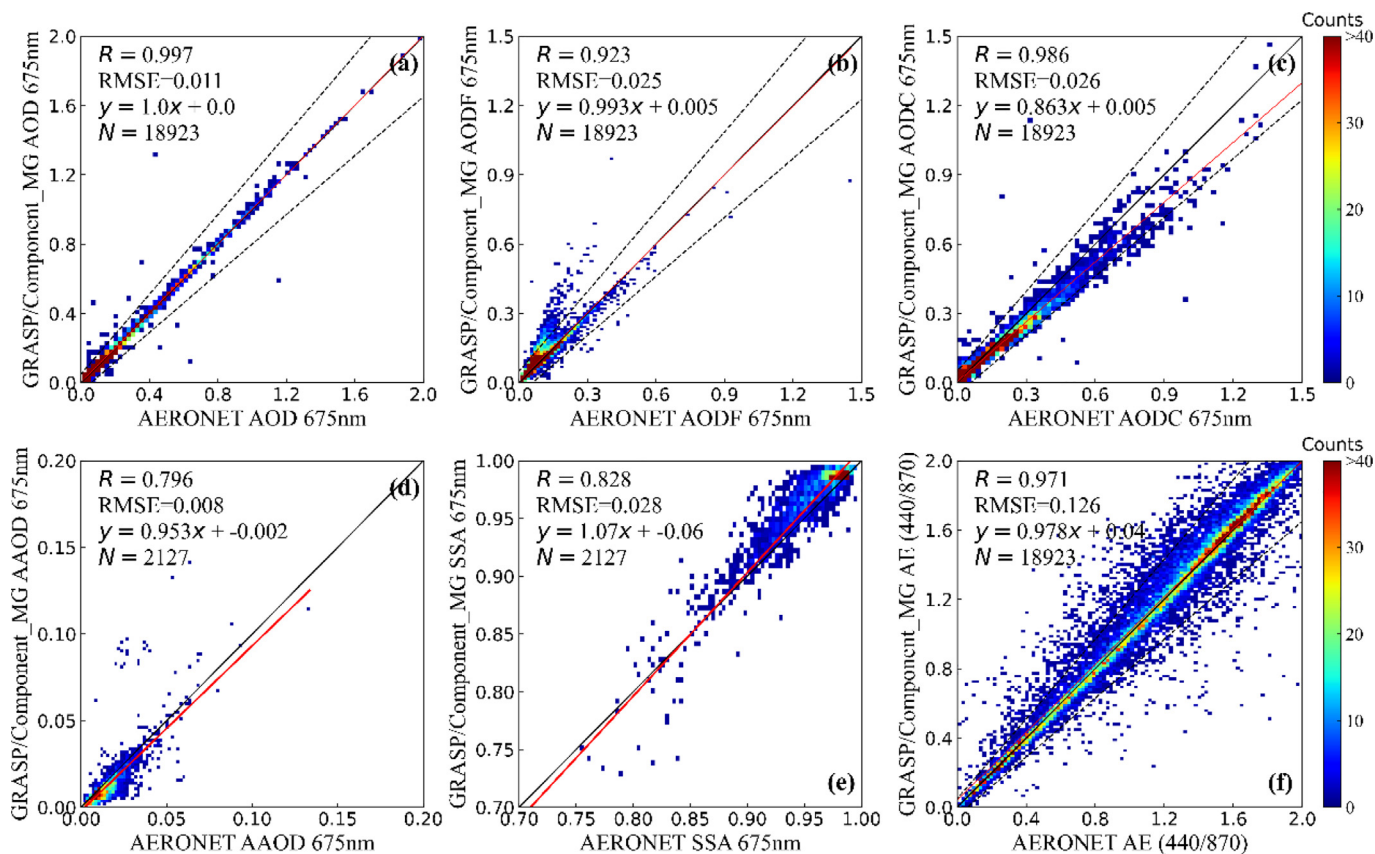

Fig. 10. Comparison of aerosol optical products derived by the GRASP/Component approach from sun photometer measurements with the corresponding AERONET standard products at all sites. The aerosol optical products are (a) AOD, (b) AODF, (c) AODC, (d) AAOD, (e) SSA, and (f) AE. The 1:1 reference line and the linear regression line are denoted by the black and red solid lines, respectively.

0.5° × 0.625° single-pixel of the MERRA-2, which is the nearest to the AERONET site, is used to represent the MERRA-2 BC product. Fig. 9 shows the intercomparison between the BC concentration retrieved by the GRASP/Component approach and MERRA-2 BC concentration for the monthly means. It can be seen that for all sites (see Fig. 9a) there is no significant variability of MERRA-2 BC concentration concentrated around 1.0 mg/m^2, while the BC concentration retrieved by GRASP/Component approach from AERONET shows a significant monthly variation with a mean absolute error (MAE) of 1.79 mg/m^2 and a mean relative error (MRE) of 63.44% that are higher than the MERRA-2 BC concentration. Specifically, the trends of BC concentration revealed by the GRASP/Component and the MERRA-2 data for the Biomass Burning (Fig. 9b) and Marine (Fig. 9e) sites are similar although there exist a few BC differences. For example, both GRASP/Component BC and MERRA-2 BC present high concentration during the biomass burning period (September–October). Noted that high MRE (811.28%) shown in Fig. 9b at biomass burning site is mainly attributed to very low BC concentration (close to 0) retrieved by GRASP/Component in June. BC concentrations shown in Fig. 9e for Marine aerosols are low but their trends have good consistency. The minimum MAE (0.78 mg/m^2) and MRE (53.19%) are found at Dust sites (Fig. 9c), which is associated with the almost same BC concentrations from March to October. The largest differences are obtained at Dust_Polution and Multi-source Urban sites (in Fig. 9d and f), which is probably because GRASP/Component BC retrievals could show the monthly variability and MERRA-2 BC products do not characterize this variability well when there are different several aerosol emission sources. Therefore, the GRASP/Component BC products show a reasonable agreement with MERRA-2 BC data.

3.2.2. Intercomparison of GRASP/component optical retrievals and AERONET products

In order to characterize the quality of the aerosol optical properties retrieved by the GRASP/Component approach from AERONET measurements, the GRASP/Component basic aerosol optical properties such as AOD, AODF, AODC, AAOD, SSA and AE are compared and evaluated by the AERONET standard products at 13 sites for different aerosol types during the period 2014–2019. Fig. 10 shows the validation of GRASP/Component aerosol optical retrievals for all sites using the corresponding AERONET standard products. Figs. A1–A5 in the appendix show the intercomparison of aerosol optical properties (AOD, AODF, AODC, AAOD and SSA) for different aerosol types. For the comparison of AOD (see Fig. 10a), we can see that the correlation coefficient R is close to 1 with a good linear regression expression (slope ~ 1, offset ~0) for all sites, and the same conclusion for each aerosol type. In addition, the RMSE is smaller than 0.02 for all sites, with the smallest RMSE of 0.003 found for the marine aerosol and the largest RMSE of 0.033 for the dust aerosol (see Fig. A1 in the appendix). The metrics for spectral AOD validation of different aerosol types are shown in Table 2. The results indicate that all wavelengths of AOD inversions show good agreement with the AERONET standard AOD products. Therefore, the GRASP/Component approach can provide spectral AOD products with the same accuracy as the AERONET standard products. As shown in Fig. 10b, the GRASP/Component AODF retrievals are in line with the AERONET products for all aerosol types. AODC products derived by the GRASP/Component approach are also consistent with the AERONET AODC for all sites (see Fig. 10c), with a correlation coefficient of R = 0.986. AAOD indicates the absorption of atmospheric particles, which is generally related to the atmospheric loading of absorbing substances such as BC, BrC and iron oxides contained in dust (Charlson et al., 1992; Dehkhoda et al., 2020; Sun et al., 2019). It can be seen that the AAOD retrievals of the GRASP/Component approach show good agreement with the AERONET standard products, with R = 0.796, slope = 0.953 and RMSE <0.01 (see Fig. 10d). The SSA, determined by the proportion of scattering AOD in the total AOD, is a key parameter for characterizing the absorption properties of aerosols and for assessing the effects of aerosols on the earth's radiation balance (Charlson et al., 1992). The results indicate that the GRASP/Component SSA retrievals have a high (taking into

Table 2
The statistics for the intercomparison of AOD derived by the GRASP/Component approach using MG effective medium approximation rules from sun photometer measurements to the corresponding AERONET standard products. The number in parentheses indicates the number of validation points.

Aerosol type	Band (nm)	R	Slope	Offset	RMSE
All sites	440 (18923)	0.997	0.998	0.002	0.013
	675 (18923)	0.997	1.000	0.000	0.011
	870 (18923)	0.997	1.005	0.000	0.011
	1020 (18923)	0.997	1.005	0.000	0.010
BB	440 (111)	1.000	0.995	0.002	0.006
	675 (111)	0.999	0.990	0.001	0.004
	870 (111)	0.996	0.988	−0.000	0.005
	1020 (111)	0.985	0.955	0.002	0.007
DU	440 (1751)	0.994	0.999	0.004	0.034
	675 (1751)	0.994	1.001	0.001	0.033
	870 (1751)	0.994	1.001	0.003	0.032
	1020 (1751)	0.994	0.999	0.004	0.031
DP	440 (4402)	0.999	0.994	0.001	0.005
	675 (4402)	0.999	0.998	0.000	0.005
	870 (4402)	0.999	1.002	0.001	0.005
	1020 (4402)	0.999	1.000	0.001	0.005
MA	440 (962)	0.999	0.986	0.003	0.004
	675 (962)	0.997	0.994	0.003	0.003
	870 (962)	0.994	1.045	−0.002	0.003
	1020 (962)	0.995	1.032	−0.002	0.002
MU	440 (11697)	0.998	0.997	0.002	0.010
	675 (11697)	0.997	0.998	0.000	0.006
	870 (11697)	0.997	1.007	−0.000	0.005
	1020 (11697)	0.997	1.004	−0.000	0.004

account rather small dynamic range of SSA) correlation (R > 0.8) and small RMSE (RMSE <0.03) when comparing to the AERONET SSA products for all sites (see Fig. 10e). The AE was determined from the fitted AOD at two different wavelengths as $AE = \frac{\ln[\tau(\lambda_1)/\tau(\lambda_2)]}{ln(\lambda_2/\lambda_1)}$. The validation of AE (440/870) derived by the GRASP/Component approach with the corresponding AERONET AE (440/870) is shown in Fig. 10f. The GRASP/Component retrieval shows high agreement with the AERONET measurements, with close statistical correlation in terms the R, slope and offset, e.g., R = 0.971, slope = 0.978, and offset = 0.04. We can see that the AE retrievals of the GRASP/Component approach are in line with the corresponding AERONET AE products.

3.2.3. Influences of component effective medium approximation on aerosol optical property retrievals

The retrieval of aerosol components requires to choose/assume the aerosol species mixing rule and the GRASP/Component approach employed a simple and extensively tested Maxwell–Garnett effective medium approximation (MG) for mixture of complex refractive indices of different aerosol species. The MG mixing rule has been widely used in many studies to retrieve aerosol components from ground-based remote sensing measurements (Schuster et al., 2005, 2009, 2016; Li et al., 2019). It is applicable to the case of insoluble small particles discretely suspended in solution (Bohren and Huffman, 1983). The MG approximation assumes that non-homogeneous particles consist of a variety of insoluble inclusions and a homogeneous matrix. Generally, the matrix can consist of water or soluble inorganic salt particles (e.g., ammonium sulfate, ammonium nitrate and sea salt) and the refractive index of the matrix is calculated using the hygroscopic properties and the ratio of soluble inorganic substances to water (Schuster et al., 2005; Li et al., 2019). As described in Li et al. (2019), two different mixing rules [MG and volume-weighted (VW) effective medium approximation] for the estimation of aerosol components can be chosen in the GRASP/Component approach. In order to quantitatively evaluate the effect of different aerosol component mixing rules on aerosol optical property inversion from ground-based sun photometer measurements, intercomparison of the monthly average aerosol optical properties
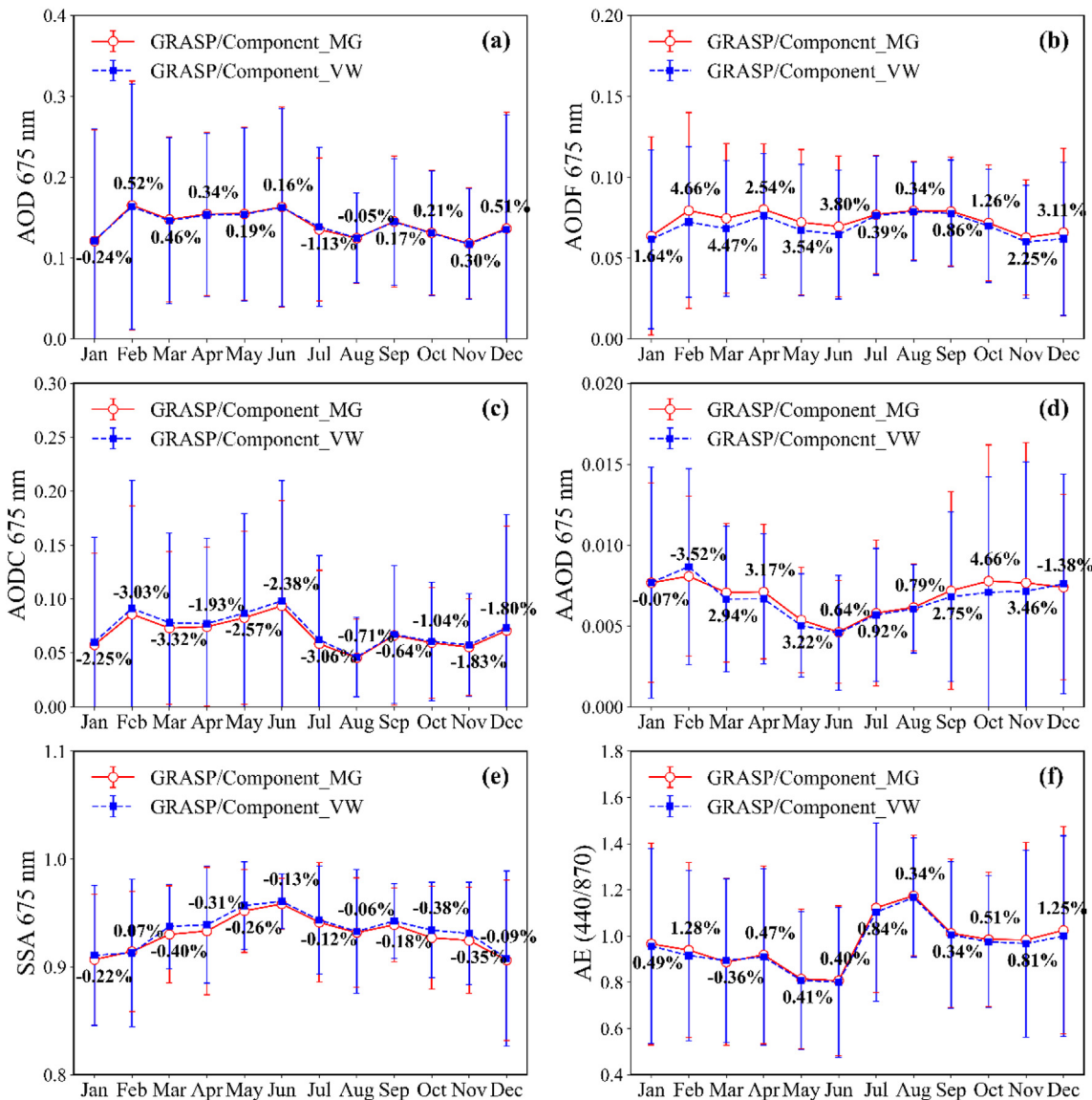
Fig. 11. Intercomparison between the monthly average aerosol optical properties derived by the MG and VW effective medium approximation rules in the GRASP/Component approach from AERONET sun photometer measurements.

derived by the MG and VW effective medium approximation rules in the GRASP/Component approach are shown in Fig. 11, and their validation metrics using AERONET products are listed in Table 3. The results

Table 3
The statistics for the intercomparison of aerosol optical properties derived by the GRASP/Component approach with MG and VW effective medium approximation rules from sun photometer measurements to the corresponding AERONET products. The number in parentheses indicates the number of validation points.

Optical property	Mixing rule	R	Slope	Offset	RMSE
AOD (675 nm)	MG (18923)	0.997	1.000	0.000	0.011
	VW (18930)	0.996	0.998	0.000	0.014
AODF (675 nm)	MG (18923)	0.923	0.993	0.005	0.025
	VW (18930)	0.911	0.903	0.008	0.025
AODC (675 nm)	MG (18923)	0.986	0.863	0.005	0.026
	VW (18930)	0.979	0.969	0.000	0.026
AAOD (675 nm)	MG (2127)	0.796	0.953	−0.002	0.008
	VW (2120)	0.669	0.974	−0.002	0.012
SSA (675 nm)	MG (2127)	0.828	1.070	−0.060	0.028
	VW (2120)	0.845	1.034	−0.026	0.025
AE (440/870)	MG (18923)	0.971	0.978	0.040	0.126
	VW (18930)	0.973	0.976	0.041	0.122

demonstrate that both MG and VW can provide highly similar aerosol optical retrievals. Specifically, the differences in optical retrievals between the MG and VW mixing rules are −1.13% to 0.52% for AOD, 0.34% to 4.66% for AODF, −3.32% to −0.64% for AODC, −3.52% to 4.66% for AAOD, −0.40% to 0.07% for SSA, and −0.36% to 1.28% for AE. The statistics shown in Table 3 indicate that both the MG and VW retrievals agree well with corresponding AERONET products, with R almost equal to 1 for AOD, AODC and AE, and being larger than 0.9 for AODF, larger than 0.8 for SSA, and about 0.7 for AAOD. The R of the AAOD retrievals are slightly low for both mixing rules listed in Table 3, which is in fact due to the presence of several outliers at the Banizoumbou site, located in the dust source area (see Fig. A4 in the appendix for MG retrieval).

4. Conclusions

This paper presents the application of GRASP/Component approach (Li et al., 2019; Dubovik et al., 2014, 2021) to a series of AERONET sun/sky photometer measurements in different locations and representing different aerosol types for the extended retrievals of aerosol components, as well as of aerosol optical properties. The intercomparison of aerosol optical

properties provided by GRASP/Component algorithm and by operational AERONET algorithm are also discussed. The main conclusions are present as follows.

The GRASP/Component approach allows the separate characterization of fine- and coarse-mode aerosol components (concentration and fraction) from ground-based sun photometer measurements. The aerosol component retrieval results able to represent well the different aerosol types including Biomass Burning (BB), Dust (DU), Marine (MA), Dust_Pollution (DP), and Multi-source Urban (MU) cases. GRASP/Component BC retrievals derived from AERONET have a reasonable agreement with MERRA-2 BC products. In addition, the results showed that the temporal variation and spatial distribution of aerosol components in the different aerosol-type regions are in general agreement with the physical expectations described by the optical parameters (AOD, FMF, AAE, SAE and SSA).

The accuracy of aerosol optical products inverted from sun photometer measurements using the GRASP/Component approach are assessed by AERONET standard products. The evaluations indicated that the optical products retrieved by the GRASP/Component approach were consistent with AERONET standard products for all considered aerosol types, e.g., the correlation coefficient for AOD, AODF, AODC, AE, SSA and AAOD is 0.997, 0.923, 0.986, 0.971, 0.828, and 0.796, respectively, and the RMSE for all spectral AODs are less than 0.02. In addition, we verified the effect of different aerosol species mixing rule assumption on retrievals of aerosol optical property. The differences between MG and VW effective medium approximation approaches were found to be within 2.3%, which demonstrates both MG and VW approaches can produce reliable aerosol optical products with same accuracy as the standard AERONET product. Therefore, the GRASP/Component approach can be applied to AERONET sun photometer measurements not only for aerosol optical properties inversion with similar accuracy as the AERONET standard products (such as AOD, AODF, AODC, AAOD, SSA and AE etc.), but also for the direct aerosol component retrievals from radiance measurements.

Declaration of Competing Interest

The authors declare that they have no known competing financial interests or personal relationships that could have appeared to influence the work reported in this paper.

Appendix A

Table A1
List of acronyms.

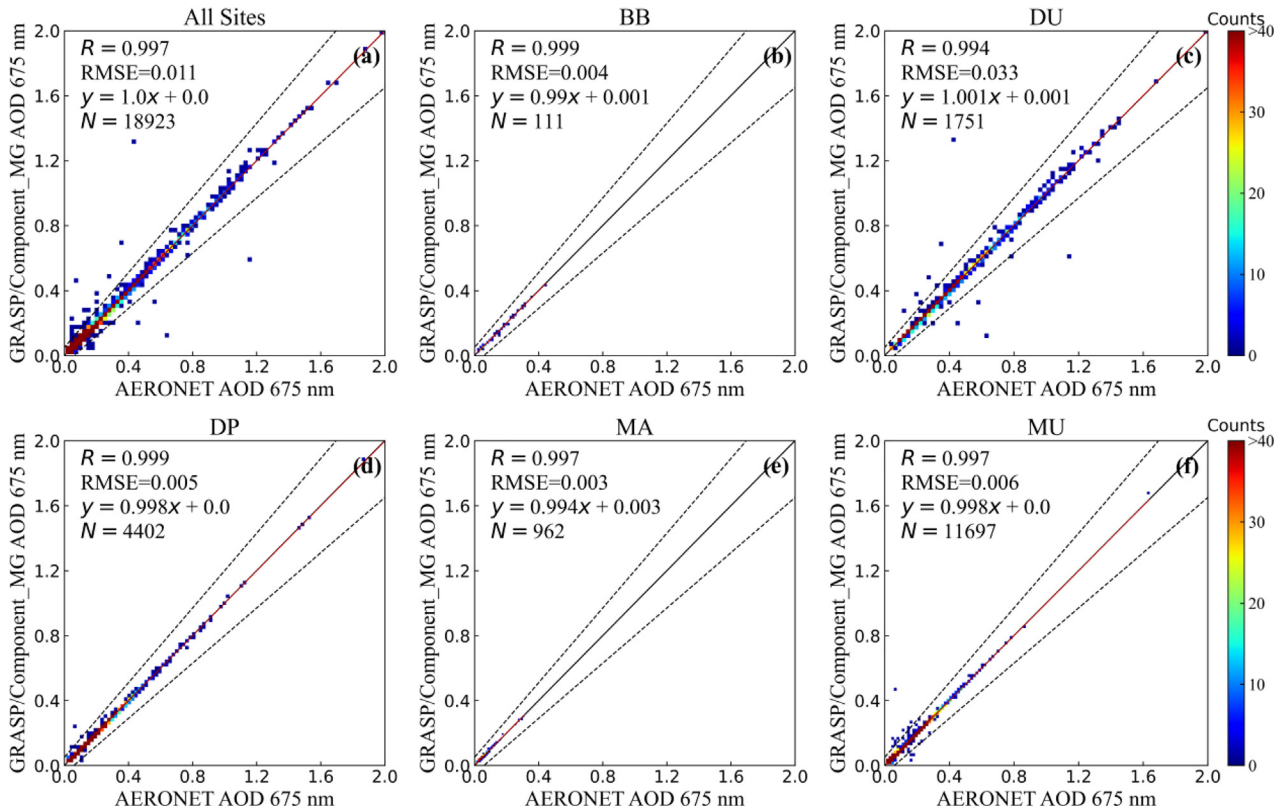| Abbreviation	Full name
AAE	Absorption Ångström exponent
AAOD	Absorption aerosol optical depth
AE	Ångström exponent
AERONET	Aeronet Robotic Network
AOD	Aerosol optical depth
AODC	Coarse-mode aerosol optical depth
AODF	Fine-mode aerosol optical depth
BB	Biomass Burning aerosol
BC	Black carbon
BrC	Brown carbon
CAI	Coarse-mode absorbing insoluble component
CARSNET	China Aerosol Remote Sensing Network
CAWC	Coarse-mode aerosol water content
CNAI	Coarse-mode non-absorbing insoluble component
CNAS	Coarse-mode non-absorbing soluble component
DP	Dust_Pollution mixing aerosol
DU	Dust aerosol
FAWC	fine-mode aerosol water content
FMF	Fine-mode fraction
FNAI	fine-mode non-absorbing insoluble component
FNAS	fine-mode non-absorbing soluble component
GEOS-5	Goddard Earth Observing System model, Version 5
GRASP	Generalized Retrieval of Atmosphere and Surface Properties
LSM	Least-squares method
MA	Marine aerosol
MAE	Mean absolute error
MERRA-2	Modern-Era Retrospective Analysis for Research and Applications, Version 2
MRE	Mean relative error
MU	Multi-source Urban aerosol
OC	Organic carbon
PHOTONS	Photométrie pour le Traitement Opérationnel de Normalisation Satellitaire
SAE	Scattering Ångström exponent
SSA	Single scattering albedo

Fig. A1. Comparison of AOD at 675 nm derived by the GRASP/Component approach along with the corresponding AERONET standard products. The 1:1 reference line and the linear regression line are denoted by the black and red solid lines, respectively.
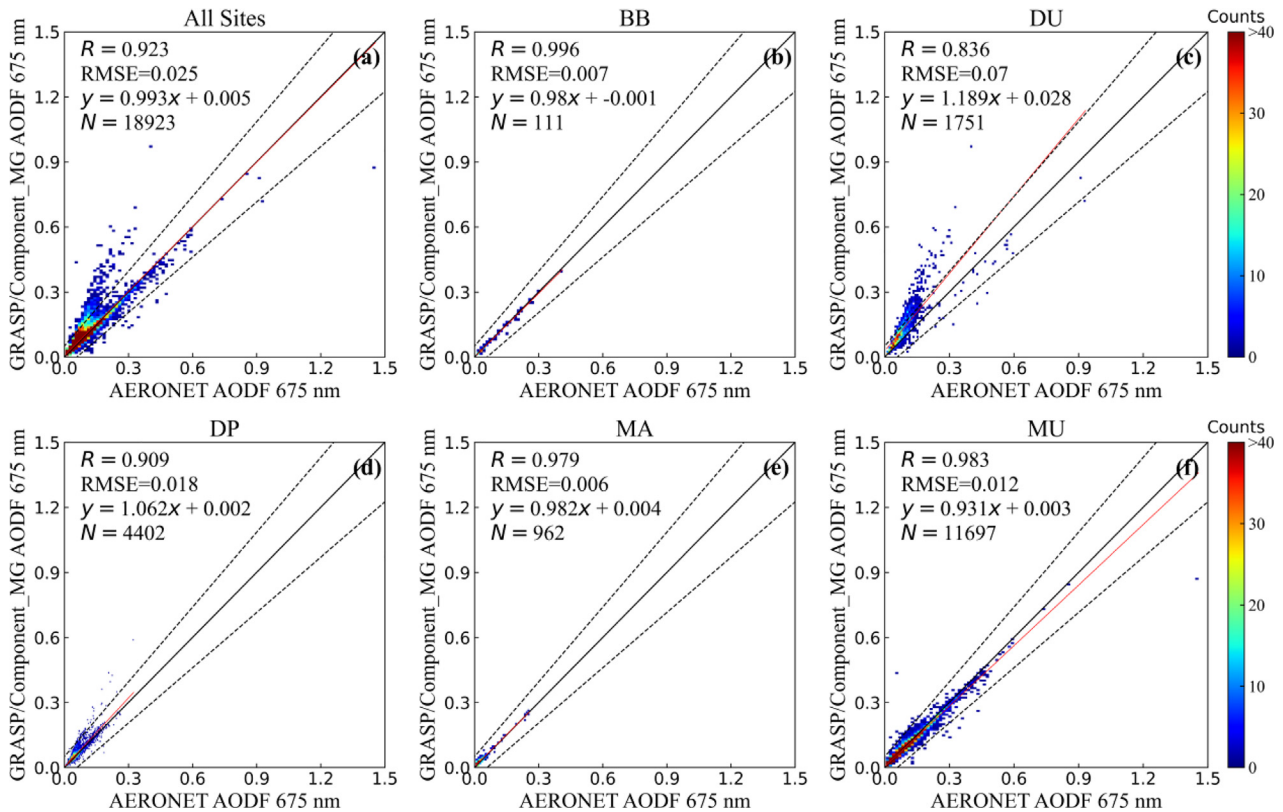

Fig. A2. Comparison of AODF at 675 nm derived by the GRASP/Component approach along with the corresponding AERONET standard products. The 1:1 reference line and the linear regression line are denoted by the black and red solid lines, respectively.

Fig. A3. Comparison of AODC at 675 nm derived by the GRASP/Component approach along with the corresponding AERONET standard products. The 1:1 reference line and the linear regression line are denoted by the black and red solid lines, respectively.
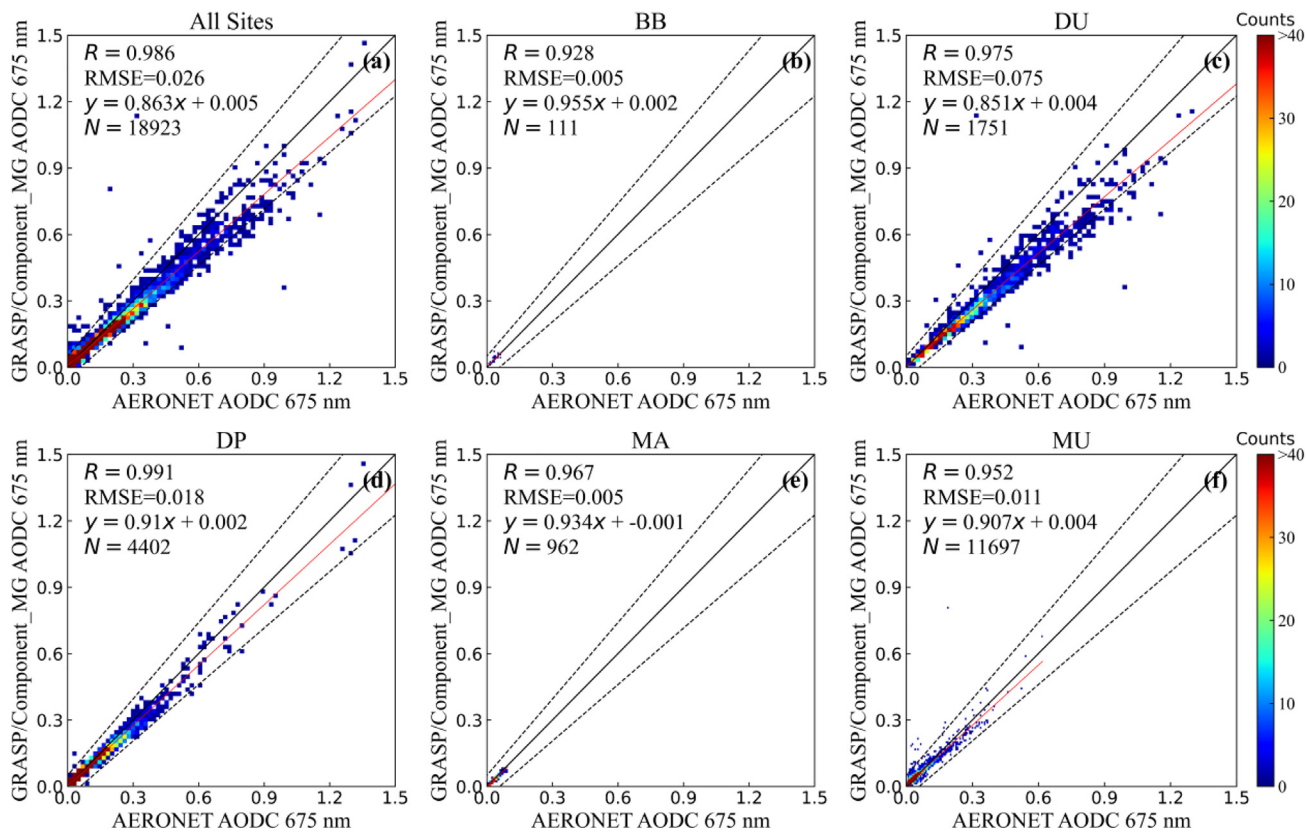

Fig. A4. Comparison of AAOD at 675 nm derived by the GRASP/Component approach along with the corresponding AERONET standard products. The 1:1 reference line and the linear regression line are denoted by the black and red solid lines, respectively.
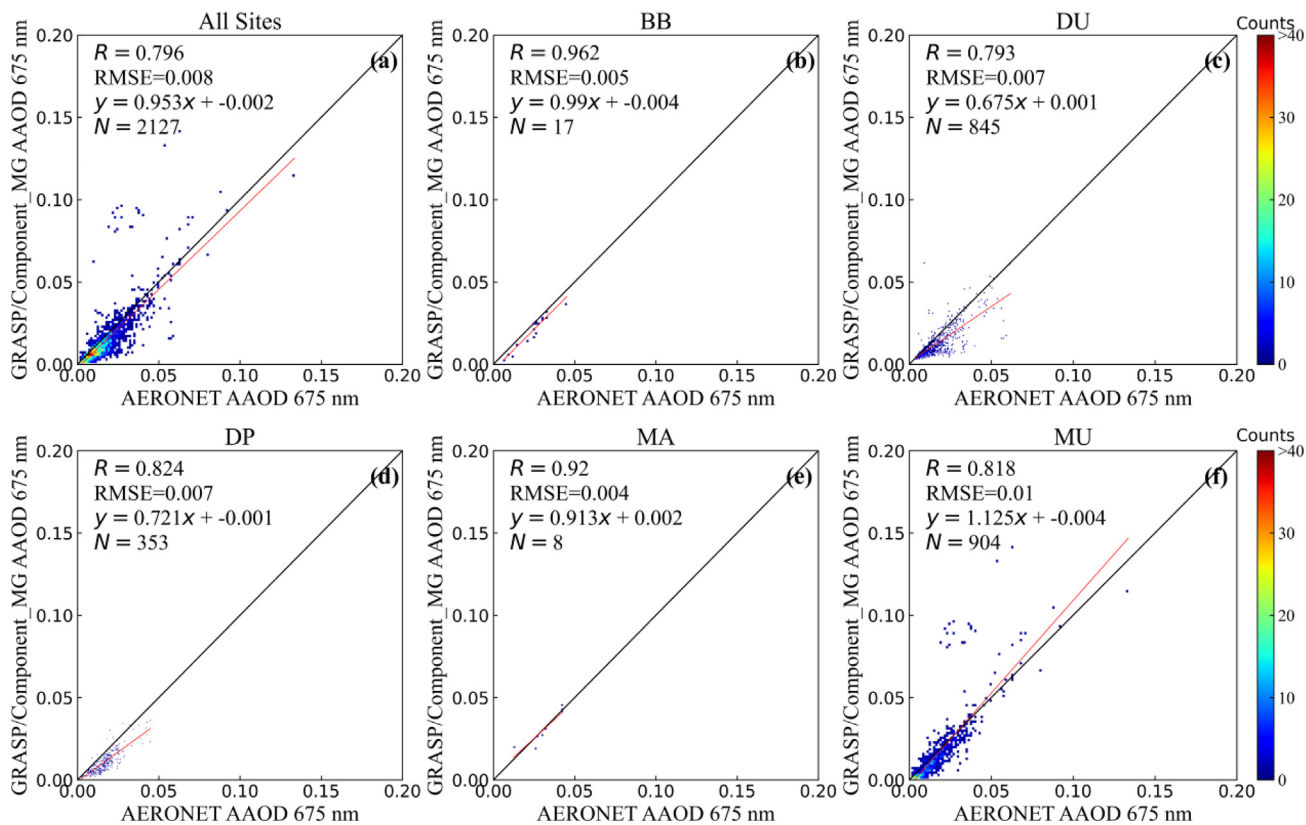
Fig. A5. Comparison of SSA at 675 nm derived by the GRASP/Component approach along with the corresponding AERONET standard products. The 1:1 reference line and the linear regression line are denoted by the black and red solid lines, respectively.
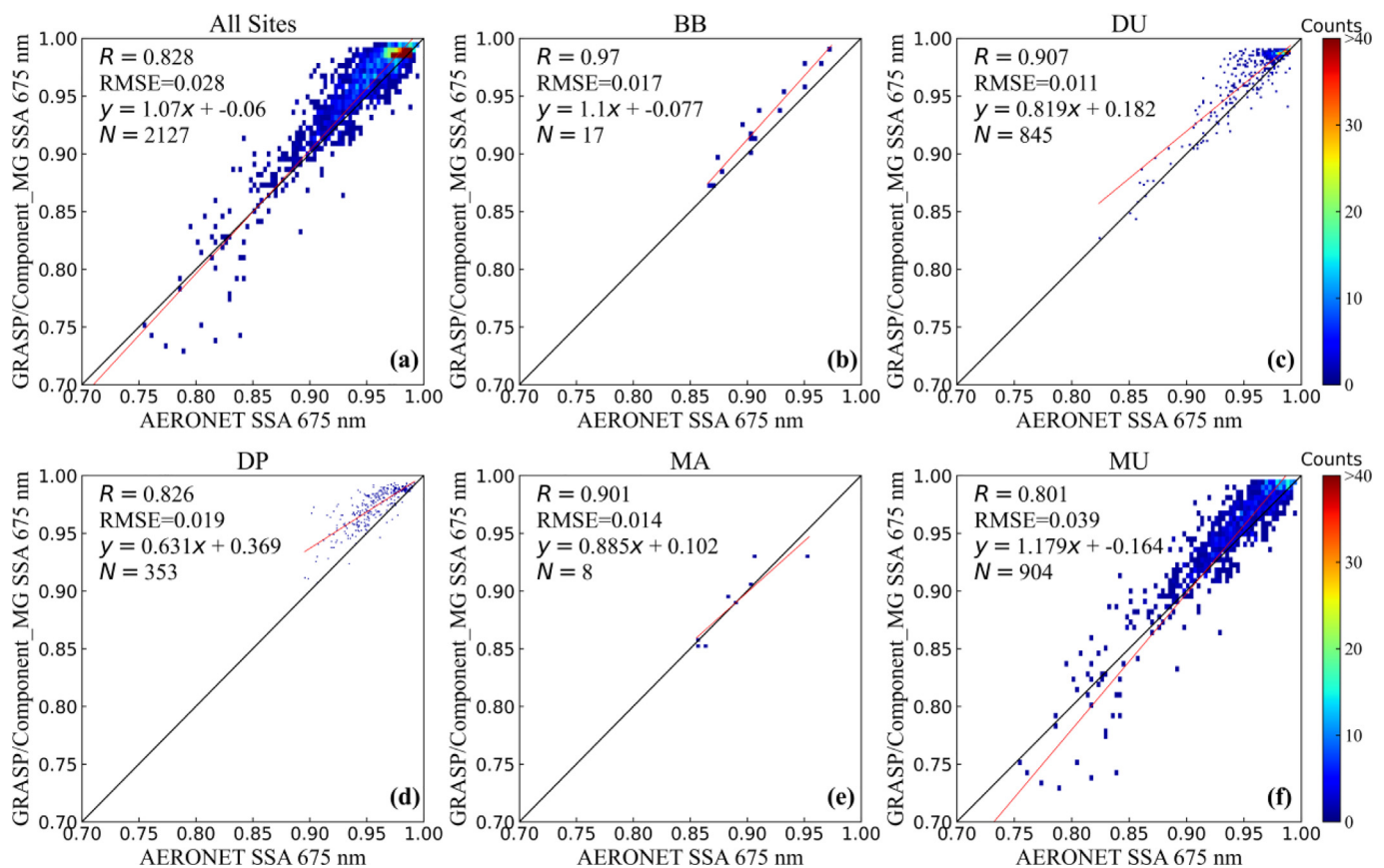
References

Hu, R.M., Blanchet, J.P., Girard, E., 2005. Evaluation of the direct and indirect radiative and climate effects of aerosols over the western Arctic. J. Geophys. Res. D: Atmos. 110, 1–10. https://doi.org/10.1029/2004JD005043.

Jin, S., Ma, Y., Zhang, M., Gong, W., Dubovik, O., Liu, B., Shi, Y., Yang, C., 2019a. Retrieval of 500 m aerosol optical depths from MODIS measurements over urban surfaces under heavy aerosol loading conditions in winter. Remote Sens. 11. https://doi.org/10.3390/rs11192218.

Jin, S., Ma, Y., Zhang, M., Gong, W., Lei, L., Ma, X., 2019b. Comparison of aerosol optical properties and associated radiative effects of air pollution events between summer and winter: a case study in January and July 2014 over Wuhan,Central China. Atmos. Environ. 218, 117004. https://doi.org/10.1016/j.atmosenv.2019.117004.

Ma, Y., Zhang, M., Jin, S., Gong, W., Chen, N., Chen, Z., Jin, Y., Shi, Y., 2019. Long-term investigation of aerosol optical and radiative characteristics in a typical megacity of Central China during winter haze periods. J. Geophys. Res.: Atmos. 124, 12093–12106. https://doi.org/10.1029/2019JD030840.

IPCC, 2013. In: Stocker, T.F., Qin, D., Plattner, G.-K., Tignor, M., Allen, S.K., Boschung, J., Nauels, A., Xia, Y., Bex, V., Midgley, P.M. (Eds.), Climate Change 2013: The Physical Science Basis. Contribution of Working Group I to the Fifth Assessment Report of the Intergovern- Mental Panel on Climate Change. Cambridge University Press, Cambridge, United Kingdom and New York, NY, USA 1535 pp.

IPCC, 2021. Summary for Policymakers. [Masson-Delmotte, V., P. Zhai, A. Pirani, S. L. Connors, C. Péan, S. Berger, N. Caud, Y. Chen, L. Goldfarb, M. I. Gomis, M. Huang, K. Leitzell, E. Lonnoy, J.B.R. Matthews, T. K. Maycock, T. Waterfield, O. Yelekçi, R. Yu and B. Zhou (eds.)]Climate Change 2021: The Physical Science Basis. Contribution of Working Group I to the Sixth Assessment Report of the Intergovernmental Panel on Climate Change. Cambridge University Press In Press.

Perlwitz, J., Seland, Ø., 2009. Evaluation of black carbon estimations in global aerosol models. Atmos. Chem. Phys. Discuss. 9, 15769–15825. https://doi.org/10.5194/acpd-9-15769-2009.

Schuster, G.L., Dubovik, O., Arola, A., 2016. Remote sensing of soot carbon - part 1: distinguishing different absorbing aerosol species. Atmos. Chem. Phys. 16, 1565–1585. https://doi.org/10.5194/acp-16-1565-2016.

Sato, M., Hansen, J., Koch, D., Lacis, A., Ruedy, R., Dubovik, O., Holben, B., Chin, M., Novakov, T., 2003. Global atmospheric black carbon inferred from AERONET. Proc. Natl. Acad. Sci. U. S. A. 100, 6319–6324. https://doi.org/10.1073/pnas.0731897100.

Van Beelen, A.J., Roelofs, G.J.H., Hasekamp, O.P., Henzing, J.S., Röckmann, T., 2014. Estimation of aerosol water and chemical composition from AERONET sun-sky radiometer measurements at cabauw, the Netherlands. Atmos. Chem. Phys. 14, 5969–5987. https://doi.org/10.5194/acp-14-5969-2014.

Bond, T.C., Charlson, R.J., Heintzenberg, L., 1998. Quantifying the emission of light-absorbing particles: measurements tailored to climate studies. Geophys. Res. Lett. 25, 337–340. https://doi.org/10.1029/98GL00039.

Streets, D.G., Gupta, S., Waldhoff, S.T., Wang, M.Q., Bond, T.C., Yiyun, B., 2001. Black carbon emissions in China. Atmos. Environ. 35, 4281–4296. https://doi.org/10.1016/S1352-2310(01)00179-0.

Dubovik, O., King, M.D., 2000. A flexible inversion algorithm for retrieval of aerosol optical properties from sun and sky radiance measurements. J. Geophys. Res. Atmos. 105, 20673–20696. https://doi.org/10.1029/2000JD900282.

Holben, B.N., Eck, T.F., Slutsker, I., Tanré, D., Buis, J.P., Setzer, A., Vermote, E., Reagan, J.A., Kaufman, Y.J., Nakajima, T., Lavenu, F., Jankowiak, I., Smirnov, A., 1998. AERONET - a federated instrument network and data archive for aerosol characterization. Remote Sens. Environ. 66, 1–16. https://doi.org/10.1016/S0034-4257(98)00031-5.

Goloub, P., Li, Z., Dubovik, O., Blarel, L., Podvin, T., Jankowiak, I., Lecoq, R., Deroo, C., Chatenet, B., Morel, J.P., Cuevas, E., Ramos, R., 2007. PHOTONS/AERONET sunphotometer network overview: description, activities, results. Proc. SPIE https://doi.org/10.1117/12.783171 69360V–69360V–15.

Che, H., Zhang, Xiaoye, Chen, H., Damiri, B., Goloub, P., Li, Z., Zhang, Xiaochun, Wei, Y., Zhou, H., Dong, F., Li, D., Zhou, T., 2009. Instrument calibration and aerosol optical depth validation of the China aerosol remote sensing network. J. Geophys. Res. Atmos. 114. https://doi.org/10.1029/2008JD011030.

Takamura, T., Nakajima, T., 2004. Overview of SKYNET and its activities. Opt. Pura Apl 37, 3303–3308.

Giles, D.M., Sinyuk, A., Sorokin, M.G., Schafer, J.S., Smirnov, A., Slutsker, I., Eck, T.F., Holben, B.N., Lewis, J.R., Campbell, J.R., Welton, E.J., Korkin, S.V., Lyapustin, A.I., 2019. Advancements in the aerosol robotic network (AERONET) version 3 database - automated near-real-time quality control algorithm with improved cloud screening for sun photometer aerosol optical depth (AOD) measurements. Atmos. Measur. Techniq. 12, 169–209. https://doi.org/10.5194/amt-12-169-2019.

Schuster, G.L., Dubovik, O., Holben, B.N., Clothiaux, E.E., 2005. Inferring black carbon content and specific absorption from aerosol robotic network (AERONET) aerosol retrievals. J. Geophys.Res. D: Atmos. 110, 1–19. https://doi.org/10.1029/2004JD004548.

Dey, S., Tripathi, S.N., Singh, R.P., Holben, B.N., 2006. Retrieval of black carbon and specific absorption over Kanpur city, northern India during 2001–2003 using AERONET data. Atmos. Environ. 40, 445–456. https://doi.org/10.1016/j.atmosenv.2005.09.053.

Arola, A., Schuster, G., Myhre, G., Kazadzis, S., Dey, S., Tripathi, S.N., 2011. Inferring absorbing organic carbon content from AERONET data. Atmos. Chem. Phys. 11, 215–225. https://doi.org/10.5194/acp-11-215-2011.

Wang, L., Li, Z.Q., Li, D.H., Li, K.T., Tian, Q.J., Li, L., Zhang, Y., Lü, Y., Gu, X.F., 2012. Retrieval of dust fraction of atmospheric aerosols based on spectra characteristics of refractive indices obtained from remote sensing measurements. Spectrosc. Spectr. Anal. 32, 1644–1649. https://doi.org/10.3964/j.issn.1000-0593(2012)06-1644-06.

Wang, L., Li, Z., Tian, Q., Ma, Y., Zhang, F., Zhang, Y., Li, D., Li, K., Li, L., 2013. Estimate of aerosol absorbing components of black carbon, brown carbon, and dust from ground-based remote sensing data of sun-sky radiometers. J. Geophys. Res. Atmos. 118, 6534–6543. https://doi.org/10.1002/jgrd.50356.

Dubovik, O., Herman, M., Holdak, A., Lapyonok, T., Tanré, D., Deuzé, J.L., Ducos, F., Sinyuk, A., Lopatin, A., 2011. Statistically optimized inversion algorithm for enhanced retrieval of aerosol properties from spectral multi-angle polarimetric satellite observations. Atmos. Measur. Techn. 4, 975–1018. https://doi.org/10.5194/amt-4-975-2011.

Dubovik, O., Lapyonok, T., Litvinov, P., Herman, M., Fuertes, D., Ducos, F., Torres, B., Derimian, Y., Huang, X., Lopatin, A., Chaikovsky, A., Aspetsberger, M., Federspiel, C., 2014. GRASP: a versatile algorithm for characterizing the atmosphere. SPIE Newsroom https://doi.org/10.1117/2.1201408.005558.

Dubovik, O., Schuster, G.L., Xu, F., Hu, Y., Bösch, H., Landgraf, J., Li, Z., 2021. Grand challenges in satellite remote sensing. Front. Remote Sens. 2. https://doi.org/10.3389/frsen.2021.619818.

Li, L., Dubovik, O., Derimian, Y., Schuster, G.L., Lapyonok, T., Litvinov, P., Ducos, F., Fuertes, D., Chen, C., Li, Z., Lopatin, A., Torres, B., Che, H., 2019. Retrieval of aerosol components directly from satellite and ground-based measurements. Atmos. Chem. Phys. https://doi.org/10.5194/acp-19-13409-2019.

Li, L., Che, H., Derimian, Y., Dubovik, O., Schuster, G.L., Chen, C., Li, Q., Wang, Y., Guo, B., Zhang, X., 2020a. Retrievals of fine mode light-absorbing carbonaceous aerosols from POLDER/PARASOL observations over east and South Asia. Remote Sens. Environ. 247, 111913. https://doi.org/10.1016/j.rse.2020.111913.

Li, L., Che, H., Derimian, Y., Dubovik, O., Luan, Q., Li, Q., Huang, X., Zhao, H., Gui, K., Zheng, Y., An, L., Sun, T., Liang, Y., 2020b. Climatology of fine and coarse mode aerosol optical thickness over east and South Asia derived from POLDER/PARASOL satellite. J. Geophys. Res.: Atmos. 125. https://doi.org/10.1029/2020JD032665 0-3.

Holben, B.N., Tanré, D., Smirnov, A., Eck, T.F., Slutsker, I., Abuhassan, N., Newcomb, W.W., Schafer, J.S., Chatenet, B., Lavenu, F., Kaufman, Y.J., Vande Castle, J., Setzer, A., Markham, B., Clark, D., Frouin, R., Halthore, R., Karneli, A., O'Neill, N.T., Pietras, C., Pinker, R.T., Voss, K., Zibordi, G., 2001. An emerging ground-based aerosol climatology: aerosol optical depth from AERONET. J. Geophys. Res. Atmos. 106, 12067–12097. https://doi.org/10.1029/2001JD900014.

Dubovik, O., Smirnov, A., Holben, B.N., King, M.D., Kaufman, Y.J., Eck, T.F., Slutsker, I., 2000. Accuracy assessments of aerosol optical properties retrieved from aerosol robotic network (AERONET) sun and sky radiance measurements. J. Geophysical Research Atmospheres 105, 9791–9806. https://doi.org/10.1029/2000JD900040.

Eck, T.F., Holben, B.N., Reid, J.S., Dubovik, O., Smirnov, A., O'Neill, N.T., Slutsker, I., Kinne, S., 1999. Wavelength dependence of the optical depth of biomass burning, urban, and desert dust aerosols. J. Geophys. Res. Atmos. 104, 31333–31349. https://doi.org/10.1029/1999JD900923.

Levy, R.C., Remer, L.A., Mattoo, S., Vermote, E.F., Kaufman, Y.J., 2007. Second-generation operational algorithm: retrieval of aerosol properties over land from inversion of moderate resolution imaging spectroradiometer spectral reflectance. J. Geophys. Res. Atmos. 112, 1–21. https://doi.org/10.1029/2006JD007811.

Lyapustin, A., Wang, Y., Korkin, S., Huang, D., 2018. MODIS collection 6 MAIAC algorithm. Atmos. Measur. Techn. Discuss. 1–50. https://doi.org/10.5194/amt-2018-141.

Bréon, F.M., Vermeulen, A., Descloitres, J., 2011. An evaluation of satellite aerosol products against sunphotometer measurements. Remote Sens. Environ. 115, 3102–3111. https://doi.org/10.1016/j.rse.2011.06.017.

Mao, Q., Zhang, H., Chen, Q., Huang, C., Yuan, Y., 2019. Satellite-based assessment of direct aerosol radiative forcing using a look-up table established through AERONET observations. Infrared Physics Technol 102, 103017. https://doi.org/10.1016/j.infrared.2019.103017.

Mélin, F., Clerici, M., Zibordi, G., Holben, B.N., Smirnov, A., 2010. Validation of SeaWiFS and MODIS aerosol products with globally distributed AERONET data. Remote Sens. Environ. 114, 230–250. https://doi.org/10.1016/j.rse.2009.09.003.

Remer, L.A., Kaufman, Y.J., Tanré, D., Mattoo, S., Chu, D.A., Martins, J.V., Li, R.R., Ichoku, C., Levy, R.C., Kleidman, R.G., Eck, T.F., Vermote, E., Holben, B.N., 2005. The MODIS aerosol algorithm, products, and validation. J. Atmos. Sci. 62, 947–973. https://doi.org/10.1175/JAS3385.1.

Kahn, R.A., Gaitley, B.J., Garay, M.J., Diner, D.J., Eck, T.F., Smirnov, A., Holben, B.N., 2010. Multiangle imaging SpectroRadiometer global aerosol product assessment by comparison with the aerosol robotic network. J. Geophys. Res. Atmos. 115. https://doi.org/10.1029/2010JD014601.

Ahn, C., Torres, O., Jethva, H., 2014. 19, 456–476. https://doi.org/10.1002/2014JD021891.

Kumar, K.R., Yin, Y., Sivakumar, V., Kang, N., Yu, X., Diao, Y., Adesina, A.J., Reddy, R.R., 2015. Aerosol climatology and discrimination of aerosol types retrieved from MODIS, MISR and OMI over Durban (29.88°S, 31.02°E),South Africa. Atmos. Environ. 117, 9–18. https://doi.org/10.1016/j.atmosenv.2015.06.058.

Dubovik, O., Holben, B., Eck, T.F., Smirnov, A., Kaufman, Y.J., King, M.D., Tanré, D., Slutsker, I., 2002. Variability of absorption and optical properties of key aerosol types observed in worldwide locations. J. Atmos. Sci. 59, 590–608. https://doi.org/10.1175/1520-0469 (2002)059<0590:voaaop>2.0.co;2.

Giles, D.M., Holben, B.N., Eck, T.F., Sinyuk, A., Smirnov, A., Slutsker, I., Dickerson, R.R., Thompson, A.M., Schafer, J.S., 2012. An analysis of AERONET aerosol absorption properties and classifications representative of aerosol source regions. J. Geophys. Res. Atmos. 117. https://doi.org/10.1029/2012JD018127.

Mallet, P.-É., Pujol, O., Brioude, J., Evan, S., Jensen, A., 2018. Marine aerosol distribution and variability over the pristine Southern Indian Ocean. Atmos. Environ. 182, 17–30. https://doi.org/10.1016/j.atmosenv.2018.03.016.

Derimian, Y., Karnieli, A., Kaufman, Y.J., Andreae, M.O., Andreae, T.W., Dubovik, O., Maenhaut, W., Koren, I., Holben, B.N., 2006. Dust and pollution aerosols over the Negev desert, Israel: properties, transport, and radiative effect. J. Geophys. Res. Atmos. 111, 1–14. https://doi.org/10.1029/2005JD006549.

Bergamo, A., Tafuro, A.M., Kinne, S., De Tomasi, F., Perrone, M.R., 2008. Monthly-averaged anthropogenic aerosol direct radiative forcing over the Mediterranean based on AERONET aerosol properties. Atmos. Chem. Phys. 8, 6995–7014. https://doi.org/10.5194/acp-8-6995-2008.

Mitchell, R.M., Forgan, B.W., Campbell, S.K., Qin, Y., 2013. The climatology of Australian tropical aerosol: evidence for regional correlation. Geophys. Res. Lett. 40, 2384–2389. https://doi.org/10.1002/grl.50403.

Kabashnikov, V., Milinevsky, G., Chaikovsky, A., Miatselskaya, N., Danylevsky, V., Aculinin, A., Kalinskaya, D., Korchemkina, E., Bovchaliuk, A., Pietruczuk, A., Sobolewsky, P., Bovchaliuk, V., 2014. Localization of aerosol sources in east-european region by back-trajectory statistics. Int. J. Remote Sens. 35, 6993–7006. https://doi.org/10.1080/01431161.2014.960621.

Chubarova, N.Y., Sviridenkov, M.A., Smirnov, A., Holben, B.N., 2011. Assessments of urban aerosol pollution in Moscow and its radiative effects. Atmos. Measur. Techn. 4, 367–378. https://doi.org/10.5194/amt-4-367-2011.

Eck, T.F., Holben, B.N., Dubovik, O., Smirnov, A., Goloub, P., Chen, H.B., Chatenet, B., Gomes, L., Zhang, X.Y., Tsay, S.C., Ji, Q., Giles, D., Slutsker, I., 2005. Columnar aerosol optical properties at AERONET sites in central eastern Asia and aerosol transport to the tropical mid-Pacific. J. Geophys. Res. D: Atmos. 110, 1–18. https://doi.org/10.1029/2004JD005274.

Giannakaki, E., Balis, D.S., Amiridis, V., Zerefos, C., 2010. Optical properties of different aerosol types: seven years of combined raman-elastic backscatter lidar measurements in Thessaloniki, Greece. Atmos. Measur. Techniq. 3, 569–578. https://doi.org/10.5194/amt-3-569-2010.

Molod, A., Takacs, L., Suarez, M., Bacmeister, J., 2015. Development of the GEOS-5 atmospheric general circulation model: evolution from MERRA to MERRA2. Geosci. Model Dev. 8, 1339–1356. https://doi.org/10.5194/gmd-8-1339-2015.

Rienecker, M.M., Suarez, M.J., Todling, R., Bacmeister, J., Takacs, L., Liu, H.-C., Gu, W., Sienkiewicz, M., Koster, R.D., Gelaro, R., Nielsen, J.E., 2008. The GEOS-5 Data Assimilation System-Documentation of Versions 5.0. 1, 5.1. 0, and 5.2. 0. NASA Technical Report 27, 118 pp.

Rienecker, M.M., Suarez, M.J., Gelaro, R., Todling, R., Bacmeister, J., Liu, E., Bosilovich, M.G., Schubert, S.D., Takacs, L., Kim, G.K., Bloom, S., Chen, J., Collins, D., Conaty, A., Da Silva, A., Gu, W., Joiner, J., Koster, R.D., Lucchesi, R., Molod, A., Owens, T., Pawson, S., Pegion, P., Redder, C.R., Reichle, R., Robertson, F.R., Ruddick, A.G., Sienkiewicz, M., Woollen, J., 2011. MERRA: NASA's modern-era retrospective analysis for research and applications. J. Clim. 24, 3624–3648. https://doi.org/10.1175/JCLI-D-11-00015.1.

Chin, M., Ginoux, P., Kinne, S., Torres, O., Holben, B.N., Duncan, B.N., Martin, R.V., Logan, J.A., Higurashi, A., Nakajima, T., 2002. Tropospheric aerosol optical thickness from the GOCART model and comparisons with satellite and sun photometer measurements. J. Atmos. Sci. 59, 461–483. https://doi.org/10.1175/1520-0469(2002)059<0461:taotft>2.0.co;2.

Colarco, P., Da Silva, A., Chin, M., Diehl, T., 2010. Online simulations of global aerosol distributions in the NASA GEOS-4 model and comparisons to satellite and ground-based aerosol optical depth. J. Geophys. Res. Atmos. 115. https://doi.org/10.1029/2009JD012820.

Torres, B., Dubovik, O., Fuertes, D., Schuster, G., Eugenia Cachorro, V., Lapyonok, T., Goloub, P., Blarel, L., Barreto, A., Mallet, M., Toledano, C., Tanré, D., 2017. Advanced characterisation of aerosol size properties from measurements of spectral optical depth using the GRASP algorithm. Atmos. Measur. Techn. 10, 3743–3781. https://doi.org/10.5194/amt-10-3743-2017.

Titos, G., Ealo, M., Román, R., Cazorla, A., Sola, Y., Dubovik, O., 2019. Retrieval of aerosol properties from ceilometer and photometer measurements : long-term evaluation with in situ data and statistical analysis at Montsec (southern Pyrenees), pp. 3255–3267.

Hu, Q., Goloub, P., Veselovskii, I., Bravo-Aranda, J.A., Elisabeta Popovici, I., Podvin, T., Haeffelin, M., Lopatin, A., Dubovik, O., Pietras, C., Huang, X., Torres, B., Chen, C., 2019. Long-range-transported Canadian smoke plumes in the lower stratosphere over northern France. Atmos. Chem. Phys. 19, 1173–1193. https://doi.org/10.5194/acp-19-1173-2019.

Tsekeri, A., Lopatin, A., Amiridis, V., Marinou, E., Igloffstein, J., Siomos, N., Solomos, S., Kokkalis, P., Engelmann, R., Baars, H., Gratsea, M., Raptis, P.I., Binietoglou, I., Mihalopoulos, N., Kalivitis, N., Kouvarakis, G., Bartsotas, N., Kallos, G., Basart, S., Schuettemeyer, D., Wandinger, U., Ansmann, A., Chaikovsky, A.P., Dubovik, O., 2017. GARRLiC and LIRIC: strengths and limitations for the characterization of dust and marine particles along with their mixtures. Atmos. Measur. Techniq. 10, 4995–5016. https://doi.org/10.5194/amt-10-4995-2017.

Chen, C.T., Cahan, B.D., 1981. Visible and ultraviolet optical properties of single-crystal and polycrystalline hematite measured by spectroscopic ellipsometry. Opt. Soc. Am. 71, 932–934.

Chen, Y., Bond, T.C., 2010. Light absorption by organic carbon from wood combustion. Atmos. Chem. Phys. 10, 1773–1787. https://doi.org/10.5194/acp-10-1773-2010.

Wang, X., Sedlacek, A.J., DeSá, S.S., Martin, S.T., Alexander, M.L., Alexander, M.L., Watson, T.B., Aiken, A.C., Springston, S.R., Artaxo, P., 2016. Deriving brown carbon from multiwavelength absorption measurements: method and application to AERONET and aethalometer observations. Atmos. Chem. Phys. 16, 12733–12752. https://doi.org/10.5194/acp-16-12733-2016.

Bahadur, R., Praveen, P.S., Xu, Y., Ramanathan, V., 2012. Solar absorption by elemental and brown carbon determined from spectral observations. Proc. Natl. Acad. Sci. U. S. A. 109, 17366–17371. https://doi.org/10.1073/pnas.1205910109.

Lack, D.A., Cappa, C.D., 2010. Impact of brown and clear carbon on light absorption enhancement, single scatter albedo and absorption wavelength dependence of black carbon. Atmos. Chem. Phys. 10, 4207–4220. https://doi.org/10.5194/acp-10-4207-2010.

Russell, P.B., Bergstrom, R.W., Shinozuka, Y., Clarke, A.D., Decarlo, P.F., Jimenez, J.L., Livingston, J.M., Redemann, J., Dubovik, O., Strawa, A., 2010. Absorption angstrom exponent in AERONET and related data as an indicator of aerosol composition. Atmos. Chem. Phys. 10, 1155–1169. https://doi.org/10.5194/acp-10-1155-2010.

Bergstrom, R.W., Pilewskie, P., Russell, P.B., Redemann, J., Bond, T.C., Quinn, P.K., Sierau, B., 2007. Spectral absorption properties of atmospheric aerosols. Atmos. Chem. Phys. 7, 5937–5943. https://doi.org/10.5194/acp-7-5937-2007.

Cazorla, A., Bahadur, R., Suski, K.J., Cahill, J.F., Chand, D., Schmid, B., Ramanathan, V., Prather, K.A., 2013. Relating aerosol absorption due to soot, organic carbon, and dust to emission sources determined from in-situ chemical measurements. Atmos. Chem. Phys. 13, 9337–9350. https://doi.org/10.5194/acp-13-9337-2013.

Jacobson, M.Z., 2001. Strong radiative heating due to the mixing state of black carbon in atmospheric aerosols. Nature 409, 695–697. https://doi.org/10.1038/35055518.

Chen, C., Dubovik, O., Fuertes, D., Litvinov, P., Lapyonok, T., Lopatin, A., Ducos, F., Derimian, Y., Herman, M., Tanré, D., Remer, L.A., Lyapustin, A., Sayer, A.M., Levy, R.C., Christina Hsu, N., Descloitres, J., Li, L., Torres, B., Karol, Y., Herrera, M., Herreras, M., Aspetsberger, M., Wanzenboeck, M., Bindreiter, L., Marth, D., Hangler, A., Federspiel, C., 2020. Validation of GRASP algorithm product from POLDER/PARASOL data and assessment of multi-angular polarimetry potential for aerosol monitoring. Earth Syst.Sci. Data 12, 3573–3620. https://doi.org/10.5194/essd-12-3573-2020.

Yang, M., Howell, S.G., Zhuang, J., Huebert, B.J., 2009. Attribution of aerosol light absorption to black carbon, brown carbon, and dust in China - interpretations of atmospheric measurements during EAST-AIRE. Atmos. Chem. Phys. 9, 2035–2050. https://doi.org/10.5194/acp-9-2035-2009.

Charlson, R.J., Schwartz, S.E., Hales, J.M., Cess, R.D., Coakley, J.A., Hansen, J.E., Hofmann, D.J., 1992. Climate forcing by anthropogenic aerosols. Science 255, 423–430. https://doi.org/10.1126/science.255.5043.423.

Dehkhoda, N., Noh, Y., Joo, S., 2020. Long-term variation of black carbon absorption aerosol optical depth from aeronet data over East Asia. Remote Sens. 12, 1–17. https://doi.org/10.3390/rs12213551.

Sun, E., Xu, X., Che, H., Tang, Z., Gui, K., An, L., Lu, C., Shi, G., 2019. Variation in MERRA-2 aerosol optical depth and absorption aerosol optical depth over China from 1980 to 2017. J. Atmos. Sol. Terr. Phys. 186, 8–19. https://doi.org/10.1016/j.jastp.2019.01.019.

Schuster, G.L., Lin, B., Dubovik, O., 2009. Remote sensing of aerosol water uptake. Geophys. Res. Lett. 36, 1–5. https://doi.org/10.1029/2008GL036576.

Bohren, C., Huffman, D., 1983. Absorption and Scattering of Light by Small Particles. Wiley https://doi.org/10.1088/0031-9112/35/3/025.